

## The Soft X-ray Aspect of Gamma-ray Bursts in the Einstein Probe Era

HAO-XUAN GAO,<sup>1</sup> JIN-JUN GENG,<sup>1,\*</sup> XUE-FENG WU,<sup>1,2,†</sup> YI-FANG LIANG,<sup>1,2</sup> FAN XU,<sup>3</sup> YONG-FENG HUANG,<sup>3,4</sup> ZI-GAO DAI,<sup>5</sup> AND WEI-MIN YUAN<sup>6</sup>

<sup>1</sup>*Purple Mountain Observatory, Chinese Academy of Sciences, Nanjing 210023, China*

<sup>2</sup>*School of Astronomy and Space Sciences, University of Science and Technology of China, Hefei 230026, China*

<sup>3</sup>*School of Astronomy and Space Science, Nanjing University, Nanjing 210023, China*

<sup>4</sup>*Key Laboratory of Modern Astronomy and Astrophysics (Nanjing University), Ministry of Education, China*

<sup>5</sup>*Department of Astronomy, School of Physical Sciences, University of Science and Technology of China, Hefei 230026, China*

<sup>6</sup>*National Astronomical Observatories, Chinese Academy of Sciences, Beijing 100101, China*

### ABSTRACT

The Einstein Probe (EP) satellite, dedicated at time-domain high-energy astrophysics and multi-messenger astronomy, was recently launched and successfully put into operation. The wide-field X-ray telescope (WXT, 0.5-4 keV) onboard has identified multiple gamma-ray burst (GRB) events, with an average duration of approximately 100 seconds. This duration is several times longer than the average duration of long gamma-ray bursts (LGRBs) detected by the Neil Gehrels *Swift* Observatory, which typically stands at around 20 seconds. Additionally, EP has detected some unknown X-ray transients whose connection to GRBs is uncertain, due to the absence of gamma-ray counterparts and efficient follow-up observation at multi-wavelengths. It is urgent to understand the physical origin of the intriguing EP GRBs. Inspired by studies of GRB 170817A, we suggest that EP GRBs may primarily consist of off-axis viewed bursts, forming a unique population among the GRB zoo. Based on LGRBs' statistical properties during the prompt phase, we explore observable properties of on-axis and off-axis LGRBs in the soft X-ray band. We predict the characteristics of several observables for these GRBs, including the duration, energy fluence, low-energy spectral index, and the slopes of Amati and Yonetoku relations, which could be tested with a larger sample of GRB events detected by EP in the future.

### 1. INTRODUCTION

Gamma-ray bursts (GRBs), the most energetic stellar explosions in the Universe, have been observed and studied for nearly 60 years. The prompt emission of GRBs is thought to come from the relativistic jet launched from the central compact remnant (Blandford & Znajek 1977; Eichler et al. 1989; Piran 2004; Kumar & Zhang 2015). It typically lasts for a few seconds (or less) and has a variable light curve consisting of several spikes. However, the radiation mechanism responsible for the prompt emission remains an open question (Zhang 2018). Both synchrotron radiation of non-thermal electrons (e.g., Mészáros et al. 1994; Tavani 1996; Zhang & Yan 2011a) and photospheric emission (e.g., Rees & Mészáros 2005; Pe'er et al. 2006; Ryde et al. 2011) have been proposed to explain the GRB prompt emission. Recently, Burgess et al. (2020) sug-

gest that synchrotron spectra from electrons in evolving (fast-to-slow) cooling regimes are capable of fitting 95% of all time-resolved spectra of the brightest long GRBs observed by the gamma-ray burst monitor (GBM: 8 keV-40 MeV) on board the NASA *Fermi* Gamma-Ray Observatory by comparing the theoretical results with observed data directly.

Before a relativistic outflow launched by the central engine can produce a successful GRB, it would inevitably propagate through the envelope or the ejected materials of the progenitor star (Bromberg et al. 2011; Berger 2014; Nagakura et al. 2014; Nakar & Piran 2016). The structure of the jet may result from the jet formation mechanism itself (van Putten & Levinson 2003; Vlahakis et al. 2003; Aloy et al. 2005), or it may arise from the breakout process as the jet penetrates the stellar materials (Levinson & Eichler 2003; Zhang et al. 2003; Lazzati 2005; Morsanyi et al. 2010; Pescalli et al. 2015; Geng et al. 2016b). Structured jets, characterized by a narrow, highly relativistic inner core surrounded by less energetic, slower-moving wings at larger angles, have

\* E-mail: jjgeng@pmo.ac.cn

† E-mail: xfwu@pmo.ac.cn

been extensively studied in the GRB community for over 20 years (e.g., Mészáros et al. 1998; Dai & Lu 2001; Lipunov et al. 2001; Zhang & Mészáros 2002a; Rossi et al. 2002; Kumar & Granot 2003). Two main types of structured jets, i.e., power-law like and Gaussian like jets, have been discussed in the literature (Granot et al. 2017; Lazzati et al. 2018; Lamb & Kobayashi 2017; Xiao et al. 2017; Kathirgamaraju et al. 2018; Meng et al. 2018; Li et al. 2019; Gao et al. 2022).

The duration of a burst is usually defined by the so-called “ $T_{90}$ ”, which is the time interval from 5 per cent to 95 per cent of the accumulated fluence. It is found that the distribution of  $T_{90}$  shows two Gaussian components with a separation line around 2 seconds in the logarithmic space (Meegan et al. 1992; Kouveliotou et al. 1993). These two components are nowadays commonly classified into the short ( $T_{90} < 2$ s) and long ( $T_{90} > 2$ s) classes, which are widely believed to originate from relativistic outflows ejected during the merger of binary compact stars and the collapse of massive stars, respectively. The number ratio of the two classes and the peak duration values of them are dependent on the energy bands and sensitivities of the instruments (e.g. Kouveliotou et al. 1993; Sakamoto et al. 2008, 2011; Paciesas & Fermi GBM Collaboration 2012; Zhang et al. 2012; Qin & Chen 2013).

On the other hand, the cosmic rate and the luminosity function (LF) of GRBs allows us to test theories about their progenitors (e.g. Liang et al. 2007; Pescalli et al. 2015). These two functions have been derived for the population of long GRBs using various methods and samples of bursts (e.g. Daigne et al. 2006; Guetta & Della Valle 2007; Firmani et al. 2004; Salvaterra & Chincarini 2007; Salvaterra et al. 2009, 2012; Wanderman & Piran 2010; Yu et al. 2015; Petrosian et al. 2015; Lan et al. 2021). Given the incomplete sampling of faint bursts and the low completeness in redshift measurements, Lan et al. (2021) carefully selected a subsample of bright *Swift* bursts to revisit the GRB LF and redshift distribution, accounting for the probability of redshift measurement. They also explored two general forms for the GRB LF: a broken power-law LF and a triple power-law LF. Their results indicate that strong redshift evolution, either in luminosity (with an evolution index of  $\delta = 1.92^{+0.25}_{-0.37}$ ) or in density ( $\delta = 1.26^{+0.33}_{-0.34}$ ), is necessary to adequately explain the observations, regardless of the assumed form of the GRB LF.

The spectrum of the prompt emission is non-thermal and often described by the so-called Band function empirically (Band et al. 1993). The Band function is characterized by three parameters, the low-energy and high-energy photon spectral indices and the peak en-

ergy ( $E_p$ ). In past years, significant efforts have been dedicated to model the shape of prompt emission spectra (e.g., Mészáros & Rees 2000; Pe’er et al. 2006; Beloborodov 2010; Uhm & Zhang 2014, 2016; Uhm et al. 2018; Geng et al. 2018b; Gao et al. 2021). GRBs display correlations between the peak energy and other observational parameters. The most famous one is the Amati relation (Amati et al. 2002). It connects the intrinsic hardness of  $E_{p,z}$ , calculated as  $E_{p,z} = E_p(1+z)$ , and the isotropic equivalent total energy of  $E_{\gamma,\text{iso}}$  emitted in gamma-rays within the 1 to  $10^4$  keV range. The index of the Amati relation is about 0.5 (Amati 2006; Nava et al. 2012; Demianski et al. 2017; Minaev & Pozanenko 2020). Another important relation, the Yonetoku relation (Yonetoku et al. 2004), shows the correlation between the intrinsic hardness of  $E_{p,z}$  and the peak luminosity of  $L_{p,\text{iso}}$ . The physical origin of these empirical relations remain under debate. Some researchers have attempted to derive the on-axis and off-axis Amati relation indices by the analytical method or by means of numerical calculations (Zhang & Mészáros 2002b; Granot et al. 2002; Eichler & Levinson 2004; Ramirez-Ruiz et al. 2005; Dado & Dar 2012; Yamazaki et al. 2004; Kocevski 2012; Mochkovitch & Nava 2015; Xu et al. 2023). Xu et al. (2023) provided a simple analytical derivation for both the Amati and Yonetoku relations within the standard fireball model, and this derivation was confirmed by numerical simulations. It was found that these relations strongly depend on the difference between the viewing angle and the jet opening angle when the jet is viewed off-axis.

Recently, the Einstein Probe (EP)<sup>1</sup> satellite, a mission by the Chinese Academy of Sciences (CAS) dedicated at time-domain high-energy astrophysics and multi-messenger astronomy, was launched and successfully put into operation (Yuan et al. 2022, 2024). The mission’s primary goals are to discover high-energy transients and monitor variable objects in the soft X-ray band, with sensitivity more than an order of magnitude greater than that of current orbiting instruments. The EP is equipped with two scientific instruments: the wide-field X-ray telescope (WXT, 0.5-4 keV) and the follow-up X-ray telescope (FXT, 0.3-10 keV). The WXT is designed to capture transients and monitor variable objects, while the FXT will perform deep follow-up observations of intriguing targets identified by the WXT

<sup>1</sup> Einstein Probe is an international mission led by the Chinese Academy of Sciences (CAS) in collaboration with the European Space Agency (ESA), the Max-Planck-Institute for extraterrestrial Physics (MPE), Germany, and the Centre National d’Études Spatiales (CNES), France.

and other facilities. The successful operation of EP is expected to generate a wealth of observational data, including soft X-ray emissions during the main burst phase of gamma-ray bursts (GRBs), X-ray-rich GRBs that gamma-ray detectors may miss, and high-redshift GRBs.

EP has detected some GRB events, including EP240219a, EP240315a, EP240617a, EP240801a, and EP240807a (Yin et al. 2024; Zhang et al. 2024; Zhou et al. 2024a,b). Notably, the soft X-ray emission duration of EP240315a reached approximately 1600 seconds (Liu et al. 2024), while other events also exhibited long durations ranging from around 70 to 300 seconds. In contrast, previous studies on the duration of long bursts have shown that the average  $T_{90}$  duration of long GRBs (LGRBs) generally falls between 10 and 20 seconds, while the duration is known to be energy-dependent (Qin & Chen 2013). Additionally, EP has detected some unknown X-ray transients that may be related to GRBs, but uncertain due to the absence of gamma-ray counterparts and efficient follow-up observation at multi-wavelengths. These transients also have long durations, such as EP240414a and EP240416a (Lian et al. 2024; Cheng et al. 2024). It may indicate that a considerable sample of underlying LGRBs with ultra-long duration in the soft X-ray band, and point to the possibility of a distinct population among GRBs.

Inspired by studies of GRB 170817A, we suggest the unique population observed by EP may primarily consist of off-axis viewed LGRBs. In this paper, we investigate properties of LGRBs in the soft X-ray band from 0.5 to 4 keV that covers the energy band of EP-WXT. Several statistical characteristics of on-axis LGRBs are re-reviewed in Section 2. The synchrotron radiation scenario and jet structure adopted in our calculations are briefly described in Section 3. In Section 4, the model parameters are constrained by matching the simulation results with the observed characteristics of on-axis GRBs, including the Amati and Yonetoku relations, the  $T_{90}$  duration, and the redshift and luminosity distribution. The properties of several observables of GRBs detected by EP are derived in Section 5. Finally, we summarize our study in Section 6. Throughout this paper a flat Lambda cold dark matter cosmological model with  $H_0 = 70 \text{ km s}^{-1} \text{ Mpc}^{-1}$ ,  $\Omega_m = 0.3$ , and  $\Omega_\Lambda = 0.7$  is adopted.

## 2. THE CHARACTERISTICS OF ON-AXIS LGRBS

Here, we briefly describe the main characteristics of on-axis LGRBs, such as the luminosity and redshift distributions, the  $T_{90}$  duration, as well as the Amati and Yonetoku relations. A detailed description of replicating

these characteristics is arranged in Section 4, while the plausible probability distributions of model parameters are determined.

### 2.1. The luminosity and redshift distributions of LGRBs

In the luminosity evolution model, the joint distribution function of redshift ( $z$ ) and luminosity ( $L$ ) for LGRBs detected by *Swift*/BAT writes as (Lan et al. 2021)

$$f(L, z) = \frac{1}{N_{\text{exp}}} \frac{c}{H_0} \frac{D_L^2(z)}{\sqrt{\Omega_\Lambda + \Omega_m (1+z)^3}} \Theta(P(L, z)) \times \frac{\psi(z)}{1+z} \phi(L, z), \quad (1)$$

where  $c$  is the speed of light,  $D_L(z)$  is the luminosity distance at  $z$ ,  $\Theta(P)$  represents the detection efficiency,  $P(L, z)$  is the peak flux of the burst,  $\psi(z)$  denotes the comoving event rate of GRBs in units of  $\text{Mpc}^{-3} \text{ yr}^{-1}$ ,  $\phi(L, z)$  is the normalized GRB luminosity function, and detailed function forms of  $\Theta(P)$ ,  $P(L, z)$ ,  $\psi(z)$ , and  $\phi(L, z)$  could be found in Lan et al. (2021). The expected number of GRBs,  $N_{\text{exp}}$ , is then given by

$$N_{\text{exp}} = \frac{\Delta\Omega T}{4\pi} \int_0^{z_{\text{max}}} \int_{\max[L_{\text{min}}, L_{\text{lim}}(z)]}^{L_{\text{max}}} \Theta(P(L, z)) \frac{\psi(z)}{1+z} \times \phi(L, z) dL dV(z), \quad (2)$$

where  $\Delta\Omega$  is the *Swift*/BAT field of view,  $T$  is the time of activity of *Swift* that covers the sample,  $L_{\text{min}}$  and  $L_{\text{max}}$  are the minimum and maximum of the luminosity,  $z_{\text{max}}$  is the maximum redshift,  $dV(z)$  is the comoving volume element,  $L_{\text{lim}}(z)$  is luminosity threshold determined by the burst redshift and BAT's flux limit, and the detailed values and expressions of them could be found in Lan et al. (2021).

### 2.2. The detected $T_{90}$ distribution of LGRBs

Tarnopolski (2016) collected 4,548 GRBs from BATSE, *Swift*, and *Fermi*, and investigated the  $\log T_{90}$  distribution of GRBs by different fitting functions. The mixture of two standard normal functions is applicable, and is adopted in this paper. For the LGRBs component we are interested in, the function is  $N(\mu, \sigma^2)$ , with  $\mu = 1.451$  and  $\sigma = 0.463$ .

### 2.3. The Amati relation and Yonetoku relation

Tsvetkova et al. (2017) presented a catalog of GRBs with known redshifts detected by the Konus-Wind (KW) experiment between 1997 and 2016. They analyzed the distribution of rest-frame GRB parameters

and confirmed the Amati and Yonetoku relations for LGRBs. Further, Tsvetkova et al. (2021) reported the results of a systematic study of GRBs with reliable redshift estimates detected simultaneously by the KW experiment (in waiting mode) and the *Swift*/BAT telescope from January 2005 to the end of 2018. In this work, 167 weak and relatively soft GRBs were added to the sample, extending the KW GRBs with known redshifts to a total of 338. The data from this expanded sample were used to fit the parameters of the Amati and Yonetoku relations for LGRBs using a Bayesian method. The derived power-law indices of the Amati and Yonetoku relations for these GRBs are 0.481 and 0.428, respectively.

### 3. THE MODEL OF GRB JETS

A GRB jet will experience internal energy dissipation, caused by internal shocks resulting from the collision between different outflow parts (Rees & Mészáros 1994; Paczynski & Xu 1994) or magnetic reconnection (Spruit et al. 2001; Zhang & Yan 2011b). Meanwhile, the electrons in the jet can be accelerated and form a non-thermal distribution in the energy space. The distribution of accelerated electrons is assumed to be a power-law of  $Q(\gamma'_e, t') = Q_0(t')(\gamma'_e/\gamma'_m)^{-p}$  for  $\gamma'_e > \gamma'_m$ , where  $Q_0$  is related to the injection rate by  $N'_{\text{inj}} = \int_{\gamma'_m}^{\gamma'_{\text{max}}} Q(\gamma'_e, t') d\gamma'_e$  (the superscript prime ' denotes the quantities in the comoving frame hereafter). These electrons will lose their energy owing to the synchrotron radiation and adiabatic cooling. Therefore, their energy distribution shows a time evolution, which is described by the continuity equation (Uhm & Zhang 2014; Geng et al. 2018b; Zhang et al. 2019; Gao et al. 2021; Gao et al. 2024) of

$$\frac{\partial}{\partial t'} \left( \frac{dN_e}{d\gamma'_e} \right) + \frac{\partial}{\partial \gamma'_e} \left[ \dot{\gamma}'_{e,\text{tot}} \left( \frac{dN_e}{d\gamma'_e} \right) \right] = Q(\gamma'_e, t'). \quad (3)$$

As the GRB jet rapidly expands with a bulk Lorentz factor of  $\Gamma$ , the toroidal-dominated magnetic field in the comoving frame decreases as  $B' = B'_0(R/R_0)^{-q}$  (Uhm & Zhang 2014), where  $R_0$  is the radius where the jet begins to produce photons and  $R$  is the radius of the expanding shell. The non-thermal electrons will be scattered by the magnetic field and emit photons with the synchrotron radiation power of  $P'_{\text{syn}}$  (Rybicki & Lightman 1979). The observed emission originates from jet elements at various latitudes, assuming a power-law struc-

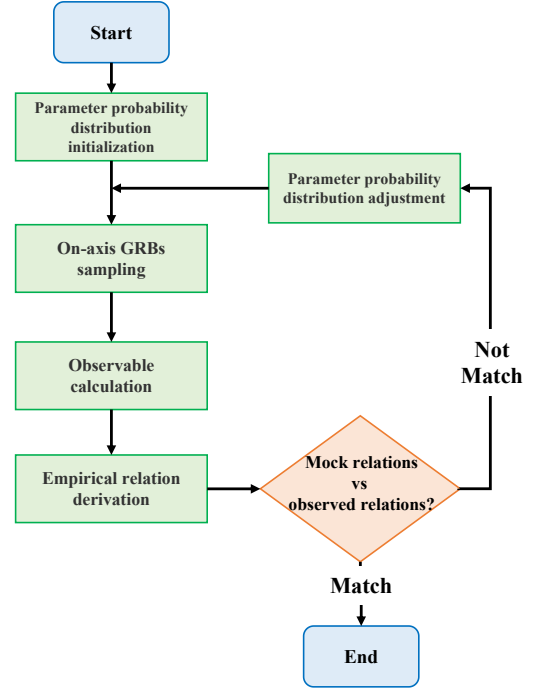


**Figure 1.** The flow chart for replicating statistical characteristics of on-axis LGRBs.

tured jet described by

$$\begin{aligned} \frac{dL}{d\Omega} &= \begin{cases} L_c, & \theta_j \leq \theta_c, \\ L_c (\theta_j/\theta_c)^{-k_L}, & \theta_c < \theta_j \leq \theta_m, \end{cases} \\ \frac{d\Gamma}{d\Omega} &= \begin{cases} \Gamma_c, & \theta_j \leq \theta_c, \\ \Gamma_c (\theta_j/\theta_c)^{-k_\Gamma} + 1, & \theta_c < \theta_j \leq \theta_m, \end{cases} \end{aligned} \quad (4)$$

where  $L_c$  and  $\Gamma_c$  are the luminosity and the Lorentz factor of the inner core, respectively.  $\theta_m$  is the maximum of the half-opening angle. The indices  $k_L$  and  $k_\Gamma$  describe the angular distribution of luminosity density  $L(\theta_j)$  and Lorentz factor  $\Gamma(\theta_j)$  within the jet cone. Note that to obtain the observed spectral flux,  $F_{\nu_{\text{obs}}}$ , it is necessary to sum up the emission from electrons over the equal-arrival-time surface (Geng et al. 2016a):

$$F_{\nu_{\text{obs}}} = \frac{1+z}{4\pi D_L^2} \int_0^{\theta_j} P'_{\text{syn}}(\nu'(\nu_{\text{obs}})) \mathcal{D}^3 \frac{\sin \theta}{2} d\theta. \quad (5)$$

### 4. MONTE CARLO SIMULATIONS

The synchrotron radiation scenario is expected to reproduce the empirical distributions and relations mentioned in Section 2. To test this idea, Monte Carlo simulations were performed. These simulations involve seven input parameters:  $\Gamma$ ,  $\gamma'_m$ ,  $N'_{\text{inj}}$ ,  $B'_0$ ,  $R_0$ ,  $t_{\text{off}}$ , and  $z$ . Here,  $t_{\text{off}}$  denotes the time in the observer frame at which electron injection ceases. Additionally, the core angle,  $\theta_c$ ,

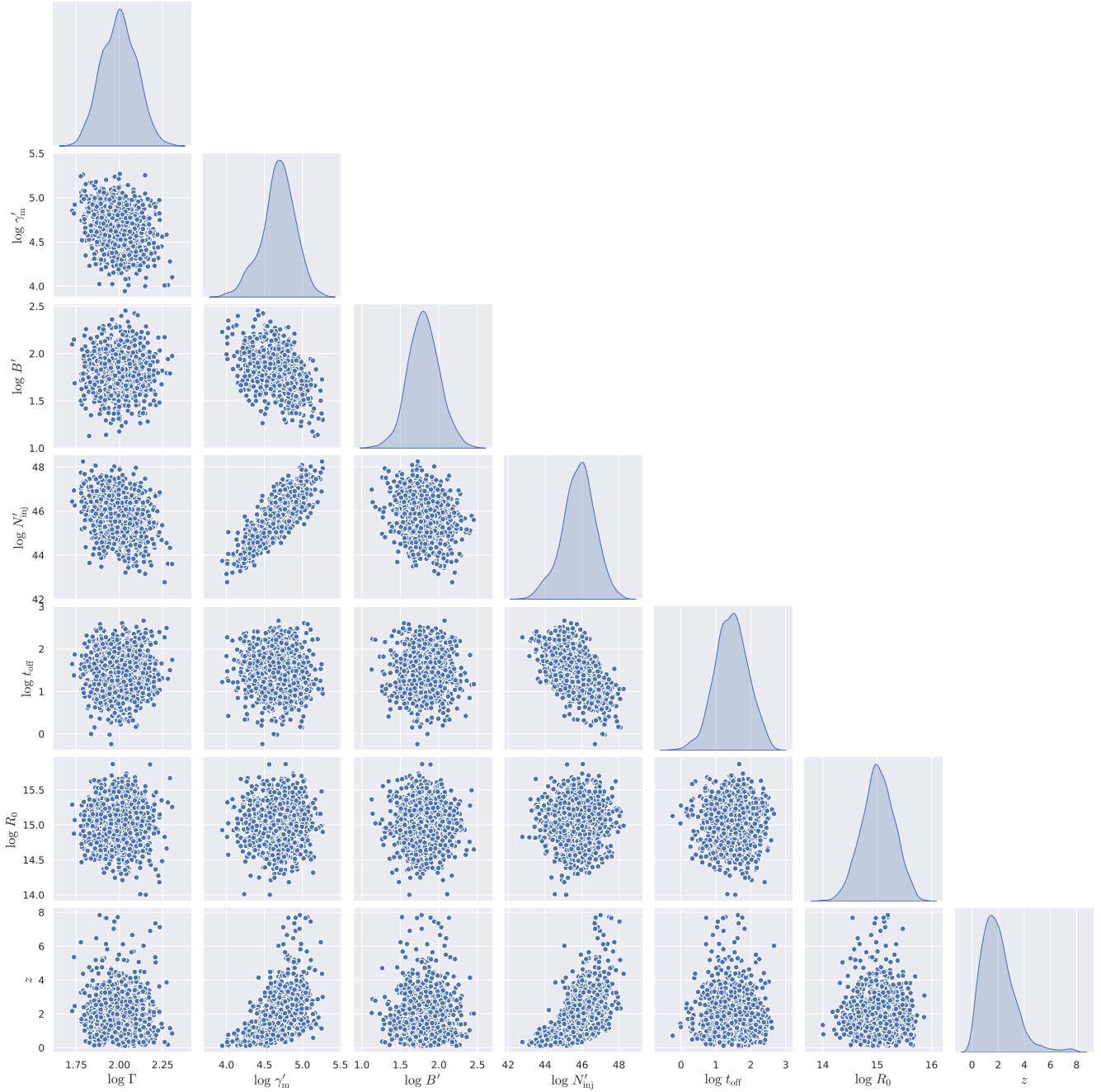


**Figure 2.** The optimal probability distribution of model input parameters, including  $\Gamma$ ,  $\gamma'_m$ ,  $N'_{\text{inj}}$ ,  $B'_0$ ,  $R_0$ ,  $t_{\text{off}}$ , and  $z$ .

is assumed to follow a normal Gaussian distribution of  $N(2.5^\circ, 1^\circ)$  (Wang et al. 2018), the viewing angle is selected from the range  $\theta_v \in [0, \theta_c]$ , and the power-law index of accelerated electrons is set to  $p = 2.3$ . During the simulations, the parameters  $k_L$  and  $k_\Gamma$  are fixed at 2 to replicate statistical characteristics of on-axis LGRBs.

Given the substantial computational cost of each calculation and the potential for strong parameter degeneracies, we did not employ a rigorous Bayesian method

for parameter constraint in this study. Instead, we manually adjusted the probability distribution of physical parameters until a satisfactory visual agreement was achieved between the simulation outcomes and the observed empirical relations. Additionally, observational data indicate that most bursts exhibit a single emission episode, though approximately (9 – 15)% of GRBs display prompt emission signatures composed of two or more episodes with intervening quiescent periods

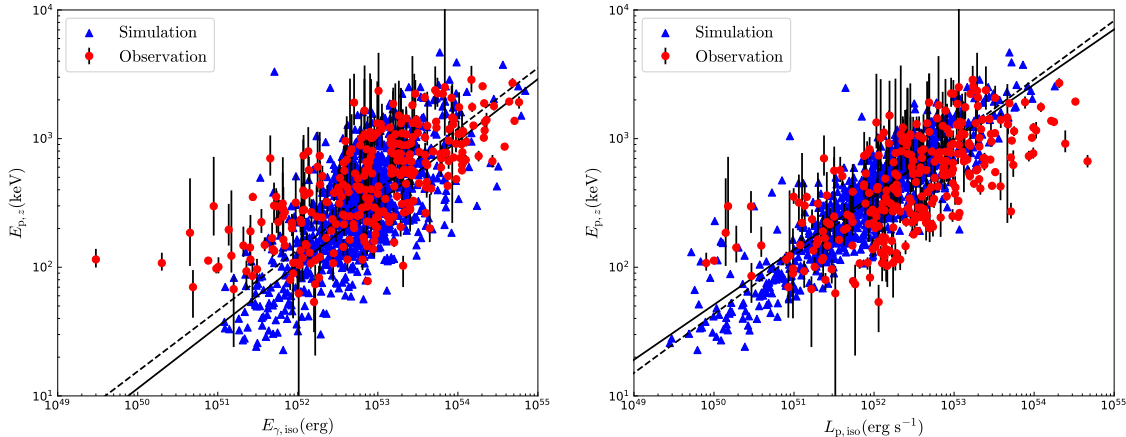


**Figure 3.** The distribution of mock and observed LGRBs in the  $L_{p,\text{iso}}-E_{p,z}$  and  $E_{\gamma,\text{iso}}-E_{p,z}$  planes. The red circle dots represent observed LGRBs from Tsvetkova et al. (2021), and the blue triangular dots show our mock results for on-axis LGRBs. The solid line and the dashed line correspond to the best-fit result for observed and mock samples, respectively.

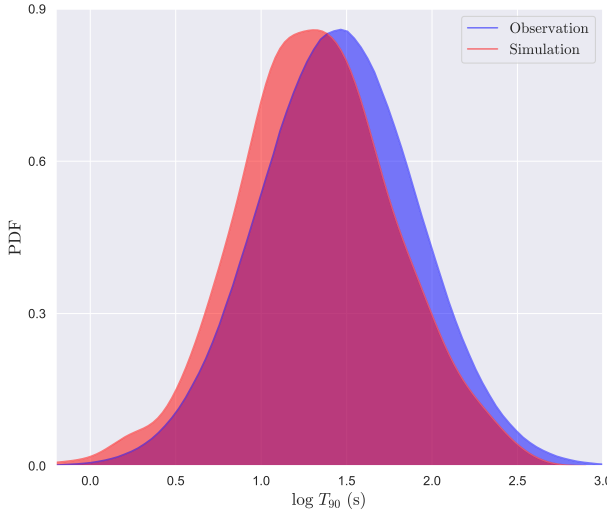


**Figure 4.** The probability distribution of  $\log T_{90}$  duration in the hard X-ray band for mock and observed LGRBs. The blue and red shadows represent observed LGRBs from Tarnopolski (2016) and mock GRBs, respectively.

(Koshut et al. 1995; Lazzati 2005; Burlon et al. 2008; Bernardini et al. 2013; Hu et al. 2014). To streamline the simulation process, we modeled long-duration bursts as consisting of a single pulse.

The simulation process (also shown in Figure 1) is as follows:

1. Generation of Input Parameters: Assuming that key parameters follow specific distributions, a set of seven input parameters are randomly generated. Each set of parameters define a mock GRB.

2. Numerical Calculation: The model is then applied to numerically calculate the corresponding values of  $E_p$ ,  $E_{\gamma,\text{iso}}$ , and  $L_{p,\text{iso}}$  for the mock GRB.

3. Sample Creation: Steps 1 and 2 are repeated to create a large sample containing 1,000 GRBs.

4. Empirical Relations: The empirical relations or distributions for the mock GRBs are derived using the Bayesian method.

5. Probability Distribution Adjustment: The empirical relations of the mock GRBs are compared with the observed empirical relations. Based on these comparisons, the initial probability distributions of input parameters are adjusted to better match the observational relations.

These five steps are repeated iteratively until the empirical relations of the mock GRBs closely align with those determined by the observation. Through this iterative process, plausible probability distributions of input parameters for the synchrotron emission scenario are determined.

#### 4.1. The generation of input parameters

Some of the seven input parameters are not mutually independent. The analysis as follow will clarify that the number of input parameters can be reduced to six and the inputs of  $\gamma'_m$  and  $N'_{\text{inj}}$  can be replaced by  $L_{p,\text{iso}}$ .

The Lorentz factor of the electrons that radiate at the GRB spectral peak energy,  $E_p$ , is denoted as  $\gamma'_m$ , which can be expressed as

$$E_p = \frac{1}{1+z} \frac{3hqeB'_0}{4\pi m_e c} \Gamma \gamma'^2, \quad (6)$$

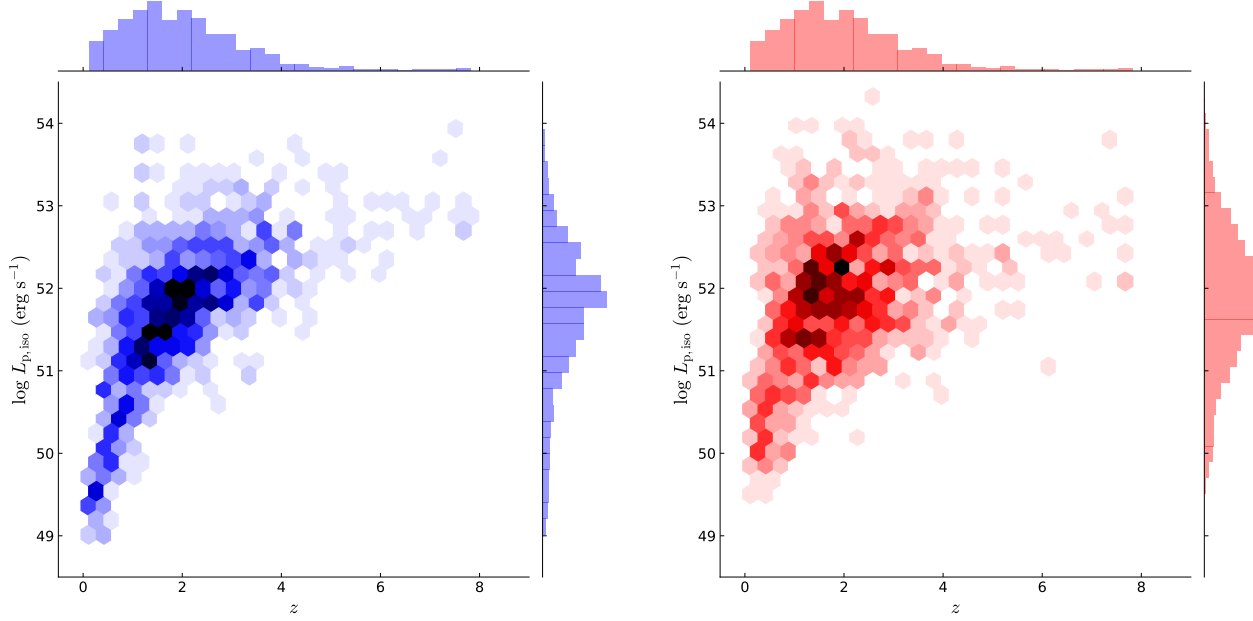


**Figure 5.** The left and right panels show the probability distribution of redshift and luminosity for observed GRBs and mock LGRBs, respectively.

where  $h$  and  $q_e$  are the Planck constant and electron charge, respectively. Solving for  $\gamma'_m$  yields

$$\gamma'_m = \sqrt{\frac{4\pi m_e c (1+z) E_p}{3h q_e B'_0 \Gamma}}. \quad (7)$$

Furthermore, the specific flux at  $E_p$  in the observer frame can be expressed as

$$F_{\nu_{\text{obs}}} = N_e \frac{\sqrt{3} q_e^3 B'_0 \Gamma}{m_e c^2} \frac{1+z}{4\pi D_L^2}, \quad (8)$$

where  $N_e$  is the total (already corrected for  $4\pi$  solid angle) number of electrons with  $\gamma'_e > \gamma'_m$  and  $D_L$  is the luminosity distance of the burst. The corresponding average injection rate of electrons,  $N'_{\text{inj}}$ , can be approximated as

$$N'_{\text{inj}} \simeq \frac{N_e}{2\Gamma\delta t_c/(1+z)}, \quad (9)$$

where  $\delta t_c = \frac{3\pi m_e c (1+z)}{\sigma_T B'^2 \gamma'_m \Gamma}$  is the radiative cooling time. Combining Equations (8) and (9), we can get

$$N'_{\text{inj}} = F_{\nu_{\text{obs}}} \frac{\sigma_T c B'_0 \gamma'_m}{\sqrt{3} q_e^3 \Gamma} \frac{2D_L^2}{3(1+z)}. \quad (10)$$

As long as the peak energy  $E_p$  and the specific flux  $F_{\nu_{\text{obs}}}$  at  $E_p$  are known,  $\gamma'_m$  and  $N'_{\text{inj}}$  can be determined by parameters of  $\Gamma$ ,  $B'_0$  and  $z$ .  $E_p$  and  $F_{\nu_{\text{obs}}}$  can always be estimated for a given  $L_{\text{p,iso}}$  and  $z$ . Considering the

empirical Yonetoku correlation, the peak energy of the time-integrated spectrum is

$$E_p = C \frac{L_{\text{p,iso}}^{0.428}}{1+z}, \quad (11)$$

where the constant of  $C$  equals  $10^{-19.712}$  keV  $\cdot$  erg  $\cdot$  s, which is determined by fitting observation data of Tsvetkova et al. (2021), and the unit of  $L_{\text{p,iso}}$  is erg  $\cdot$  s  $\cdot$  s $^{-1}$ .

We further assume the shape of the photon spectrum in the observer frame takes the form of (Band et al. 1993)

$$N(E) = \begin{cases} A \left( \frac{E}{100\text{keV}} \right)^\alpha \exp \left( -\frac{E}{E_0} \right), & E < (\alpha - \beta)E_0, \\ A \left[ \frac{(\alpha - \beta)E_0}{100\text{keV}} \right]^{\alpha - \beta} \exp(\beta - \alpha) \left( \frac{E}{100\text{keV}} \right)^\beta, & E \geq (\alpha - \beta)E_0, \end{cases} \quad (12)$$

in which the values of the low and high spectral indices are  $\alpha = -1$  and  $\beta = -2.3$ , respectively, and  $A$  is the normalization of the spectrum. Then  $F_{\nu_{\text{obs}}}$  can be estimated by

$$F_{\nu_{\text{obs}}} = AhE_p N(E_p), \quad (13)$$

where  $A = L_{\text{p,iso}}/4\pi D_L^2 / \int_{1/(1+z)}^{10^4/(1+z)} EN(E) dE$ .

Thus, the seven input parameters initially mentioned in this subsection can be reduced to six:  $\{z, L_{\text{p,iso}}, \Gamma, B'_0, R_0, t_{\text{off}}\}$ . These input parameters are assumed to follow specific distributions. The redshift ( $z$ ) and peak luminosity ( $L_{\text{p,iso}}$ ) is assumed to follow the probability

distribution of Equation (1). The bulk Lorentz factor ( $\Gamma$ ), the magnetic field ( $B'_0$ ) and the jet radius ( $R_0$ ) are assumed to follow the log-normal distribution, indicating that their logarithms are normally distributed according to  $N(\mu, \sigma^2)$ . The parameter  $t_{\text{off}}$ , which approximately represents the duration of the burst, is assumed to conform to the detected  $T_{90}$  distribution of LGRBs mentioned in Subsection 2.2.

#### 4.2. The generation of observables

For each group of input parameters, the isotropic bolometric emission energy, the bolometric peak luminosity, the peak energy of the time-integrated spectrum, and the  $T_{90}$  duration in the hard X-ray band are calculated. The isotropic emission energy is defined as (Bloom et al. 2001)

$$E_{\gamma, \text{iso}} = \frac{4\pi D_L^2 \int_0^{\Delta T} dt_{\text{obs}} \int_{\nu_1/(1+z)}^{\nu_2/(1+z)} F_{\nu_{\text{obs}}} d\nu_{\text{obs}}}{1+z}, \quad (14)$$

where  $\Delta T$  is the time during which the observed  $\gamma$ -ray flux surpasses the detection threshold ( $\sim 2 \times 10^{-8}$  erg cm $^{-2}$  s $^{-1}$ ) of the *Swift*/BAT, with an exposure time set at 2 seconds. The frequencies  $\nu_1$  and  $\nu_2$  correspond to the frequencies of the 10 keV and 10 $^4$  keV photons, respectively. The bolometric peak luminosity  $L_{\text{p,iso}}$  is the peak value of the isotropic emission luminosity  $L$  given by

$$L = 4\pi D_L^2 \int_{\nu_1/(1+z)}^{\nu_2/(1+z)} F_{\nu_{\text{obs}}} d\nu_{\text{obs}}. \quad (15)$$

The peak energy,  $E_{\text{p}}$ , of the time-integrated spectrum is obtained by fitting the time-integrated flux  $\int_0^{\Delta T} F_{\nu_{\text{obs}}} dt_{\text{obs}}$  with the Band function as defined in Equation (12), where  $E_{\text{p}} = (\alpha + 2)E_0$ . To compute the  $T_{90}$  duration, we calculate the photon count spectrum by using  $C(\nu_{\text{obs}}) = \frac{F_{\nu_{\text{obs}}}}{h\nu_{\text{obs}}}$ , where the unit of  $C(\nu_{\text{obs}})$  is cts  $\cdot$  s $^{-1}$   $\cdot$  Hz $^{-1}$ .  $T_{90}$  is defined by

$$T_{90} = t_{95} - t_5, \quad (16)$$

where the times  $t_5$  and  $t_{95}$  are defined such that

$$\begin{aligned} \frac{\int_0^{t_5} dt_{\text{obs}} \int_{\nu_1/(1+z)}^{\nu_2/(1+z)} C(\nu_{\text{obs}}) d\nu_{\text{obs}}}{\int_0^{\Delta T} dt_{\text{obs}} \int_{\nu_1/(1+z)}^{\nu_2/(1+z)} C(\nu_{\text{obs}}) d\nu_{\text{obs}}} &= 5\%, \\ \frac{\int_0^{t_{95}} dt_{\text{obs}} \int_{\nu_1/(1+z)}^{\nu_2/(1+z)} C(\nu_{\text{obs}}) d\nu_{\text{obs}}}{\int_0^{\Delta T} dt_{\text{obs}} \int_{\nu_1/(1+z)}^{\nu_2/(1+z)} C(\nu_{\text{obs}}) d\nu_{\text{obs}}} &= 95\%. \end{aligned} \quad (17)$$

#### 4.3. The optimal probability distribution of input parameters

After numerous iterations, we identified the optimal probability distribution of input parameters, which are illustrated in Figure 2. The corresponding probability distributions of the mock GRBs are presented in Figures 3-5. As shown in Figure 3, the distribution of mock GRBs in the  $L_{\text{p,iso}}-E_{\text{p,z}}$  and  $E_{\gamma, \text{iso}}-E_{\text{p,z}}$  planes aligns well with those of the observed LGRBs. The slopes of Amati and Yonetoku relations for mock GRBs are 0.473 and 0.421, which are close to the corresponding slope values of 0.481 and 0.428 of the observed LGRBs. The probability distribution of the  $T_{90}$  duration in the hard X-ray band for mock GRBs is exhibited in Figure 4. The average  $T_{90}$  duration for mock GRBs is about 20 s, which is close to the observed average value of 28 s for LGRBs. A comparison of the probability distributions of redshift and luminosity between the mock LGRBs and the observed LGRBs is shown in Figure 5. Although the median luminosity of the mock GRBs is slightly higher than that of the observed GRBs, the distribution range of the mock GRBs in the  $z\text{-log}L_{\text{p,iso}}$  plane closely matches that of the observed GRBs.

### 5. OBSERVABLES IN THE SOFT X-RAY ENERGY BAND

In Section 4, we constraint the plausible probability distribution of the input parameters based on the statistical characteristics of currently observed on-axis LGRBs. In this section, Monte Carlo simulations were conducted to investigate several observables in the soft X-ray band (0.5-4 keV) for LGRBs, including the  $T_{90}$  duration, energy fluence, and low-energy spectral index. The Amati and Yonetoku relations and the detection rate for EP LGRBs are also discussed. Furthermore, we explore the dependence of observables on different jet structures, while the structure parameters  $k_L$  and  $k_F$  are assumed to be in a range of [-2, -4].

#### 5.1. Duration and energy fluence

The observer's line of sight has an equal probability of pointing to any direction within the solid angle  $[0, 4\pi]$ . Assuming that the jet axis direction corresponds to  $\theta_v = 0$ , the viewing angle  $\theta_v$  follows the probability distribution

$$f(\theta_v) = \frac{1}{2} \sin \theta_v, \quad (18)$$

where  $\theta_v \in [0, \pi]$ . However, when the viewing angle is too large, detecting the burst becomes challenging. For a uniform jet with sharp edges, the ratio of off-axis to on-axis  $E_{\gamma, \text{iso}}$  is given by (Granot et al. 2017):

$$\frac{E_{\gamma, \text{iso}}(\theta_v)}{E_{\gamma, \text{iso}}(0)} \approx \frac{(\Gamma \theta_j)^2}{(\Gamma \theta_v)^6}, \quad \theta_v > 2\theta_j. \quad (19)$$

Assuming  $E_{\gamma, \text{iso}}(0) \approx 10^{54}$  erg,  $E_{\gamma, \text{iso}}(5\theta_c)$  becomes less than  $10^{48}$  erg when typical values for  $\Gamma$  ( $\sim 100$ ) and  $\theta_c$  ( $\sim 2.5^\circ$ ) are used. High-energy bursts viewed at a large angle, such as  $5\theta_c$ , would thus appear as low-luminosity GRBs to the detector. Therefore, in the simulations for off-axis GRBs, the viewing angle  $\theta_v$  is restricted to the range  $[0, 5\theta_c]$ . In this section, we define a burst as an on-axis GRB if the viewing angle is less than the core angle of the GRB jet, and as an off-axis GRB if the viewing angle is greater than the core angle. It is expected that GRBs observed by EP will include both on-axis and off-axis bursts. Assuming that the core angle is  $2.5^\circ$  and the maximum viewing angle is  $12.5^\circ$ , off-axis bursts will account for  $\sim 99\%$  of the total bursts by a detector. However, simulations reveal that off-axis bursts actually account for  $\sim 90\%$  of EP GRBs, as the flux of many off-axis bursts falls below EP's detection threshold.

The probability distribution of  $T_{90}$  duration in the soft X-ray band for on-axis GRBs and EP GRBs is shown in Figure 6. As electrons with energy of  $\gamma'_m m_e c^2$  cool down, the characteristic frequency of their synchrotron radiation will cross the hard X-ray band and then the lower energy bands. Consequently, the hard X-ray emission reaches peak flux before the soft X-ray emission and also attenuates sooner. This results in a slightly longer average  $T_{90}$  duration in the soft X-ray energy band compared to the hard X-ray band. For on-axis GRBs, the average  $T_{90}$  duration in the soft X-ray band is approximately 80 s.

On the other hand, the duration time  $\Delta t'$  of the burst in the comoving frame can be related to the observer's time  $\Delta t_{\text{obs}}$  by

$$\Delta t_{\text{obs}} \approx (1+z)\Gamma(1-\beta \cos \bar{\theta})\Delta t', \quad (20)$$

where  $\bar{\theta}$  is the average angle between the motion direction of the jet elements and the line of sight of the observer. Assuming  $\theta_c = 2.5^\circ$  and  $\theta_v = 5^\circ$ , the average angle  $\bar{\theta}$  is calculated by

$$\bar{\theta} = \frac{\int_0^{2\pi} \int_{\theta_v}^{\theta_c} \arccos(\sin \theta_v \sin \theta \cos \phi + \cos \theta_v \cos \theta) \sin \theta d\theta d\phi}{2\pi \int_{\theta_v}^{\theta_c} \sin \theta d\theta}. \quad (21)$$

For the on-axis case,  $\bar{\theta}_{\text{on}}$  is approximately  $1.6^\circ$ , while for the off-axis case,  $\bar{\theta}_{\text{off}}$  is about  $5.2^\circ$ . The ratio of the observed time  $t_{\text{obs}}(5.2^\circ)$  to  $t_{\text{obs}}(1.6^\circ)$  is given by

$$\frac{t_{\text{obs}}(\bar{\theta}_{\text{off}})}{t_{\text{obs}}(\bar{\theta}_{\text{on}})} = \frac{1 - \beta \cos \bar{\theta}_{\text{off}}}{1 - \beta \cos \bar{\theta}_{\text{on}}} \approx 8, \quad (22)$$

using a typical value of  $\Gamma \approx 100$ . Simulations indicate that the average  $T_{90}$  duration for EP bursts are found to

lie within the ranges of  $\sim [140 \text{ s}, 168 \text{ s}]$  for various power indices associated with the jet structure, as illustrated in the right panel of Figure 6. Note that the hard X-ray photons observed by the on-axis observer will appear as soft X-ray photons to the off-axis observer, due to the Doppler effect. The duration ratio of EP bursts to *Swift* bursts fall within the range of  $\sim [7, 8]$ , which is in agreement with the estimate provided by the analytical equation.

The possibility distribution function of  $T_{90}$  duration for on-axis bursts and EP bursts is presented in Figure 7. Owing to the beaming effect, only a small portion of photons can be detected by an off-axis observer, resulting in a lower median energy fluence ( $\sim 10^{-9} \text{ erg} \cdot \text{cm}^{-2}$ ) for mock EP LGRBs compared to mock on-axis LGRBs. Changes in the structure parameters of GRB jets have slight influence on the average energy fluence of EP LGRBs.

## 5.2. Low-energy spectral index

The low-energy spectral index  $\alpha$  ( $F_\nu \propto \nu^\alpha$ ) is also calculated. As shown in Figure 8, the  $\alpha$  values of on-axis LGRBs are primarily distributed around  $-0.5$ , which is expected in the fast-cooling regime of the synchrotron scenario. In our model, the surrounding magnetic field of the jet decreases, and the fast-cooling electrons can have a harder energy spectrum, resulting in  $\alpha$  values greater than  $-0.5$  (Uhm & Zhang 2014; Geng et al. 2018a).

The observed soft X-ray emission (of  $h\nu_{\text{obs}}$ ) corresponds to the higher energy radiation (of  $(1+z)h\nu_{\text{obs}}/\mathcal{D}$ ) in the comoving frame, which has a softer energy spectral index. A larger observing angle leads to a smaller Doppler factor of

$$\mathcal{D} \approx 1/[\Gamma(1 - \beta \cos \bar{\theta})], \quad (23)$$

and the photon energy in the comoving frame, which corresponds to the observed soft X-ray emission, increases and approaches that of the hard X-ray. Consequently, the low-energy spectral index of the observed spectrum decreases. As illustrated in Figure 8, the average value of  $\alpha$  for mock EP LGRBs is approximately  $-0.6$ , which is lower than that for mock on-axis LGRBs, and is almost independent of the structure parameters of GRB jets.

Notably, the distribution of the low-energy spectral index of mock GRBs may differ from that of actually observed events. The statistics of  $\alpha$  are in contention with a synchrotron origin for GRBs (Preece et al. 1998). This contention was eased by detailed treatment of the cooling processes of electrons (Derishev et al. 2001; Daigne et al. 2011; Uhm & Zhang 2014; Zhao et al. 2014; Geng et al. 2018b), such as taking into account the syn-

chrotron self-Compton (SSC) cooling and the decreasing of the jet magnetic field. However, the SSC cooling process is ignored in this paper in order to reduce the consumption of computing resources. The careful treatment of the cooling processes should be performed in future investigations.

### 5.3. The Amati and Yonetoku relations for off-axis LGRBs

The mock distribution of EP LGRBs in the  $L_{p,\text{iso}}-E_{p,z}$  and  $E_{\gamma,\text{iso}}-E_{p,z}$  planes is shown in Figure 9. This figure indicates that most EP LGRBs should be low-luminosity GRBs, with  $E_{\gamma,\text{iso}}$  values below  $10^{48}$  erg. Only a small fraction of them fall within the  $10^{49}\text{--}10^{55}$  erg range due to the beaming effect. Xu et al. (2023) provide a simple analytical derivation of the Amati and Yonetoku relations for both on-axis and off-axis GRBs. Their findings show that these relations depend on the value of  $\theta_v - \theta_c$  when the jet is viewed off-axis. They also suggest that the slopes of both the Amati and Yonetoku relations for off-axis GRBs are lower than those for on-axis GRBs, and a similar result can be observed in the upper left and upper right panels in Figure 9. For EP bursts, the best-fit Amati relation is  $E_p \propto E_{\gamma,\text{iso}}^{0.266}$ , and the best-fit Yonetoku relation is  $E_p \propto L_{p,\text{iso}}^{0.246}$ , with the indices  $k_L$  and  $k_\Gamma$  fixed at 4. For various power indices associated with the jet structure, the optimal slopes of the Amati and Yonetoku relations are found to lie within the ranges of [0.22, 0.35] and [0.22, 0.31], respectively.

### 5.4. The detection rate of EP GRBs

We now estimate detection rate of LGRBs for EP, especially for off-axis LGRBs. The average number of LGRBs detected by *Swift* each year is approximately 70 (Lan et al. 2021). Assuming that LGRBs observed by *Swift* are primarily on-axis bursts, approximately 700 on-axis LGRBs and nearly 7,000 off-axis LGRBs are expected to occur across the celestial sphere each year. If the detection sensitivity limit is not taken into account, the detector with a field of view of  $3,600 \text{ deg}^2$ , similar to that of EP, will catch nearly 500 off-axis bursts and 50 on-axis bursts a year. In practice, however, only about 60% of off-axis bursts exceed the EP detection threshold, while the majority of on-axis bursts do. Consequently, EP is expected to detect  $\sim 370$  LGRBs per year, with  $\sim 90\%$  of these being off-axis events, as illustrated in Figure 10.

We also examine the number of off-axis LGRBs detected by EP that have gamma-ray counterparts. Monte Carlo simulations indicate a  $\sim 10\%$  probability that an off-axis burst observed by EP would also be detectable by *Fermi* with a  $5\sigma$  detection threshold of  $\sim 0.5$

$\text{ph cm}^{-2} \text{ s}^{-1}$ , and approximately 30 off-axis bursts per year are expected to be jointly detected by both EP and *Fermi*.

In the estimation, we assume an ideal operational mode for the sky survey conducted by both EP and *Fermi*. However, in reality, the sky survey is occasionally interrupted by other observation programs, causing some GRBs to be missed by EP and *Fermi*. Additionally, the two satellites follow different orbits and do not always observe the same regions of the sky. As a result, a burst detected by EP may not be observed by *Fermi*. On the other hand, in the absence of the afterglow observation, it is hard to identify a burst as an off-axis GRB (Alexander et al. 2018; Kasliwal et al. 2017; Kathirgamaraju et al. 2018; Li et al. 2019). Thus, the actual off-axis LGRB detection rate will be lower than our simulation result.

For our estimation, we use the  $5\sigma$  detection threshold for *Fermi*. However, some bursts with fluxes below this threshold may still be confirmed as GRBs. Additionally, an X-ray transient missed by *Fermi* could potentially be detected by KW and be identified as a GRB. Therefore, the probability that an off-axis burst observed by EP is confirmed as a GRB may be higher than our estimated value.

As discussed in Subsection 5.1, the average  $T_{90}$  duration in the soft-Xray band for off-axis LGRBs ranges from approximately 140 to 168 seconds, depending on the jet structure parameters, and is comparable to the average duration of GRBs detected by EP. Moreover, off-axis LGRBs constitute roughly 90% of the total LGRBs observed by EP. These findings suggest that the GRBs detected by EP may be primarily off-axis LGRBs. This conclusion can be further tested with a larger sample of GRB events detected by EP in the future, by comparing the predicted average value of various observables, such as duration, energy fluence, low-energy spectral index, and the slopes of the Amati and Yonetoku relations.

## 6. CONCLUSIONS AND DISCUSSION

EP has identified some GRB events, with a average duration of  $\mathcal{O}(100)$  seconds, several times longer than the average duration of LGRBs observed by *Swift*. It is urgent to understand the physical origin of the intriguing EP GRBs. Based on statistical characteristics of LGRBs accumulated in the past, we constrain the physical parameters of GRB jets within the synchrotron emission scenario and investigate the distributions of observables in the soft X-ray band for LGRBs detected by EP, including the duration, energy fluence, and low-energy spectral index. The Amati and Yonetoku rela-

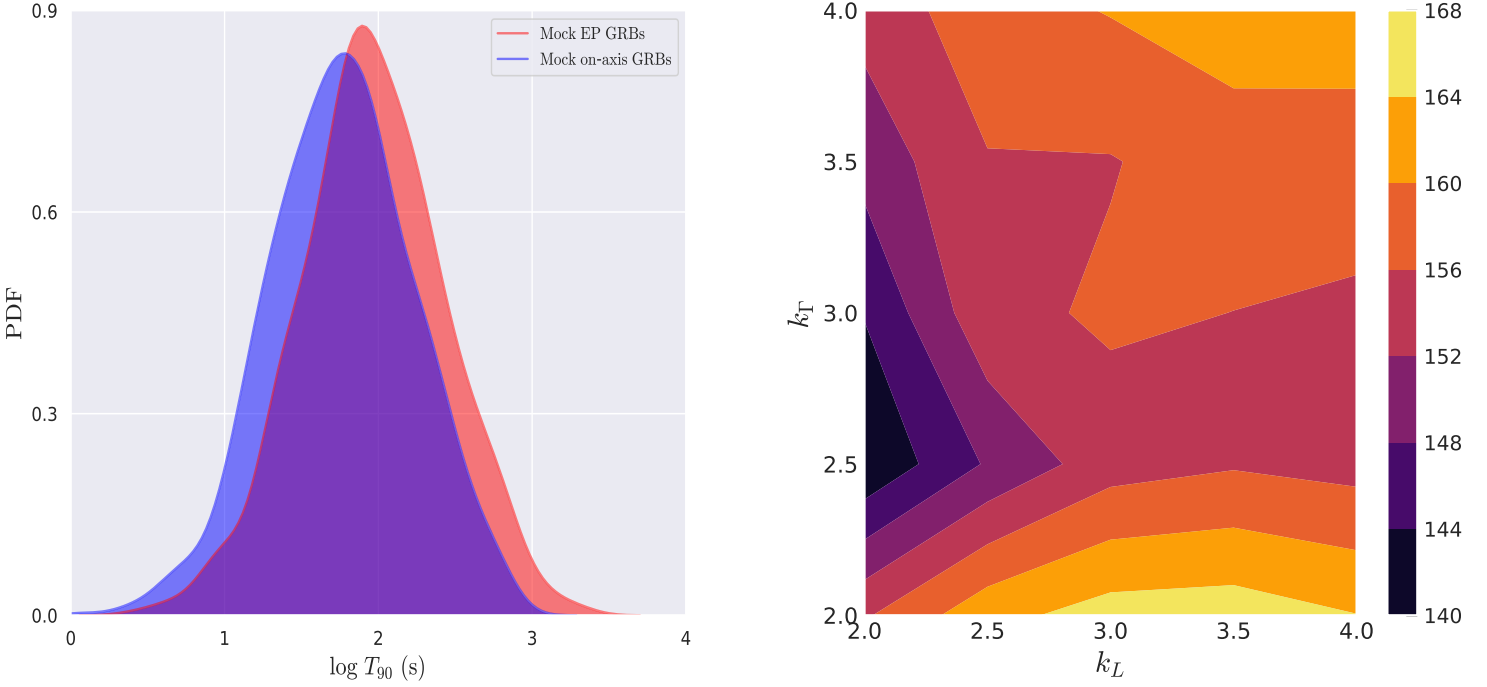


**Figure 6.** The  $T_{90}$  duration of EP GRBs predicted by Monte Carlo simulations in the soft X-ray band. Left panel: The mock probability distribution of  $\log T_{90}$  duration for mock on-axis LGRBs and mock EP LGRBs, with the indices  $k_L$  and  $k_T$  fixed at 4. The blue and red shadows represent on-axis LGRBs and EP LGRBs, respectively. Right panel: The dependence of the average  $T_{90}$  duration for mock LGRBs of EP on the jet structures.

tions for EP LGRBs are also studied. Additionally, the dependence of observables on different jet structures is explored. We suggest that the new population with particularly long durations observed by EP may primarily consist of off-axis LGRBs.

Assuming a viewing angle of within  $5\theta_c$ , we examine the observables in the soft X-ray band during the main burst for both on-axis and off-axis LGRBs. For on-axis LGRBs, the average  $T_{90}$  duration is approximately 80 s. A larger viewing angle results in a greater average angle between the motion direction of jet elements and the observer's line of sight. Due to the Doppler effect, off-axis LGRBs exhibit a longer  $T_{90}$  duration. As off-axis LGRBs account for  $\sim 90\%$  of burst observed by EP, the average duration of EP bursts falls within the ranges of  $\sim [140, 168]$  s for various power-law indices associated with the jet structure. The duration ratio of LGRBs observed by EP in the soft X-ray band to on axis LGRBs observed in the gamma-ray and hard X-ray band is  $\sim 8$ .

Monte Carlo simulations reveal that the average energy fluence of on-axis LGRBs is about  $10^{-6}$  erg  $\cdot$  cm $^{-2}$ . Due to the beaming effect, only a small portion of photons are detected by an off-axis observer, resulting in

a lower average energy fluence of approximately  $10^{-9}$  erg  $\cdot$  cm $^{-2}$  for EP LGRBs. We find that the structure parameters of GRB jets have little influence on the average energy fluence of EP LGRBs.

The values of low-energy spectral index,  $\alpha$ , for the on-axis LGRBs are primarily distributed around -0.5, which is expected in the fast-cooling regime of the synchrotron scenario. In our scenario, the surrounding magnetic field of the jet decreases, and the fast-cooling electrons can have a harder energy spectrum, with  $\alpha$  that can be greater than -0.5. For the LGRBs detected by EP, the average value of  $\alpha$  is approximately -0.6, and  $\alpha$  exhibits a broad distribution range from -0.9 to 0, and is almost independent of the structure parameters of GRB jets.

The Amati and Yonetoku relations for EP LGRBs are also explored. It is seen that the EP LGRBs form a unique population in the  $E_{\gamma,\text{iso}} - E_{p,z}$  and  $L_{p,\text{iso}} - E_{p,z}$  diagrams. Due to the beaming effect, only a small fraction of EP LGRBs fall within the  $10^{49} - 10^{55}$  erg range. The slopes of both the Amati and Yonetoku relations for these bursts are lower than those for on-axis LGRBs. For different structure parameters of GRB jets, the opti-

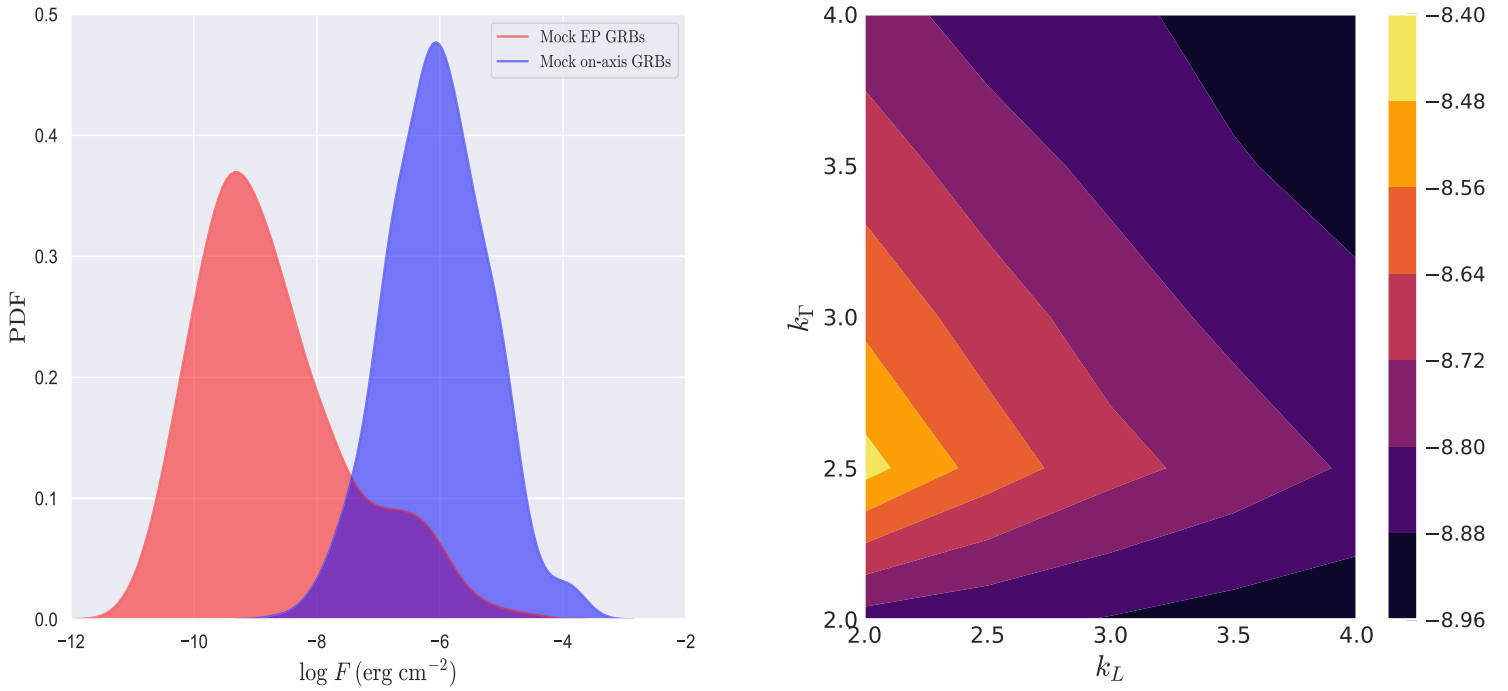


**Figure 7.** The energy fluence of EP GRBs predicted by Monte Carlo simulations in the soft X-ray band. Left panel: The mock probability distribution of the energy fluence ( $F$ ) for on-axis LGRBs and EP LGRBs, with the indices  $k_L$  and  $k_T$  fixed at 4. The blue and red shadows represent on-axis LGRBs and EP GRBs, respectively. Right panel: The dependence of the average  $\log F$  for mock LGRBs of EP on the jet structures.

mal slopes of Amati and Yonetoku relations are found to lie within the ranges of  $\sim[0.22, 0.35]$  and  $\sim[0.22, 0.31]$ , respectively. Based on the average number of LGRBs detected by *Swift* each year, the optimistic detection rate of LGRBs by EP/WXT is approximately 370 per year, among which the off-axis LGRBs account for approximately 90%. We also estimate the number of off-axis LGRBs detected by EP that have gamma-ray counterparts, and approximately 30 off-axis bursts per year are expected to be jointly detected by both EP and *Fermi*. As more GRB data from EP is collected, this hypothesis can be tested by directly comparing these simulated features, including the distribution of  $T_{90}$  duration and energy fluence, the slopes of the Amati and Yonetoku relations, with the observational results.

In the main text, a power-law structured jet is assumed, and it is found that various jet parameters have only a minor influence on the distribution of observables for off-axis bursts. It is expected that Monte Carlo simulations based on a Gaussian jet will yield similar results to those obtained in the power-law structured jet case.

In the literature, it has been argued that there are many orphan afterglows in the sky, which could be

produced by relativistic outflows whose motion is not pointed toward us (Rhoads 1997). These outflows are essentially off-axis GRB jets. They do not show up as GRBs simply because our line of sight is not on the axis. However, their afterglow may still be observable when the outflow is significantly decelerated at late stages so that softer photons are emitted into a much wider solid angle. Such afterglows are called orphan afterglows because they are not associated with any GRBs. Observing these orphan afterglows may potentially help measure the beaming angle of normal GRBs (Mészáros et al. 1999), but no firm detection of these fascinating phenomena has been established yet despite extensive observational efforts (Ho et al. 2022). We argue that the X-ray transients detected by EP may be the early counterpart of orphan afterglows. It is thus solicited that these X-ray transients be followed and monitored by large telescopes at multi-wavelengths, which may hopefully lead to the discovery of orphan afterglows. Note that orphan afterglows may also be produced by “failed GRBs”, i.e. isotropic baryon-contaminated fireballs with the Lorentz factor much less than 100 (Huang et al. 2002). These two kinds of orphan afterglows, i.e., off-axis ones and failed-

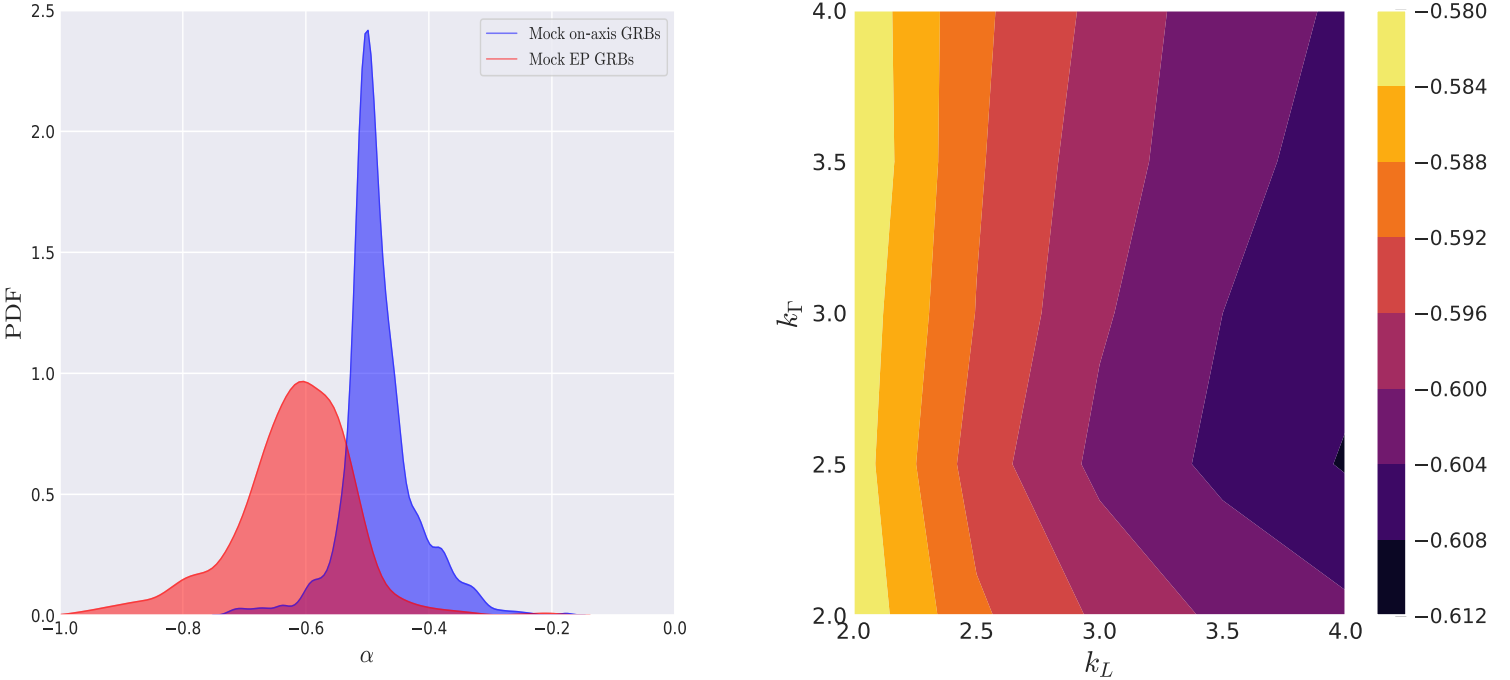


**Figure 8.** The low-energy spectral index  $\alpha$  ( $F_\nu \propto \nu^\alpha$ ) predicted by Monte Carlo simulations for EP GRBs. Left panel: The mock probability distribution of  $\alpha$  for on-axis LGRBs and EP LGRBs, with the indices  $k_L$  and  $k_T$  fixed at 4. The blue and red shadows represent on-axis LGRBs and EP LGRBs, respectively. Note that the mock probability distribution for LGRBs is scaled by a factor of 0.2. Right panel: The dependence of the average  $\alpha$  for mock LGRBs of EP on the jet structures.

GRB-induced events, could be discriminated by examining their decaying behaviors at late stages (Huang et al. 2002).

Extragalactic fast X-ray transients (FXTs), short-duration ( $\sim$ ks) X-ray flashes of unknown origin, may also be linked to orphan afterglows. Wichern et al. (2024) have explored the possible connection between FXTs and the afterglows of off-axis, merger-induced GRBs. Their analysis suggests that a slightly off-axis viewing angle of  $\theta_{\text{obs}} \approx (2.2 - 3)\theta_c$  and a structured jet are necessary to explain the shallow temporal indices ( $|\alpha| \leq 0.3$ ) observed in FXT light curves, which can not be accounted for a uniform jet at any viewing angle. Future observations of FXTs by EP will help clarify the potential connection between GRBs and FXTs and may eventually identify the progenitors of some FXTs.

The long duration in the soft X-ray band may also hint at the intrinsic characteristics of some LGRBs themselves. Except for ultrarelativistic jets launched from the GRB central engine sufficiently discussed in the literature, there is growing evidence that the mildly relativistic jets (Sun et al. 2024b) or weak jets (Sun et al. 2024a) could play significant roles. Radiation from these

jets may be concentrated in the soft X-ray band and obscured by emissions from strong jets, making it difficult to identify them in the prompt and afterglow phase. The fraction of these intrinsic long GRBs in EP GRBs remains highly uncertain and invokes further studies.

The successful launch of EP in early 2024 opened up a new window into the transient X-ray sky. EP is expected to yield a substantial amount of observational data in the near future, including soft X-ray emissions during the main burst of GRBs, X-ray-rich GRBs that gamma-ray detectors may miss, and high-redshift GRBs. This will help us to unveil the physical origins of GRBs and shed light on the mysteries of the early universe.

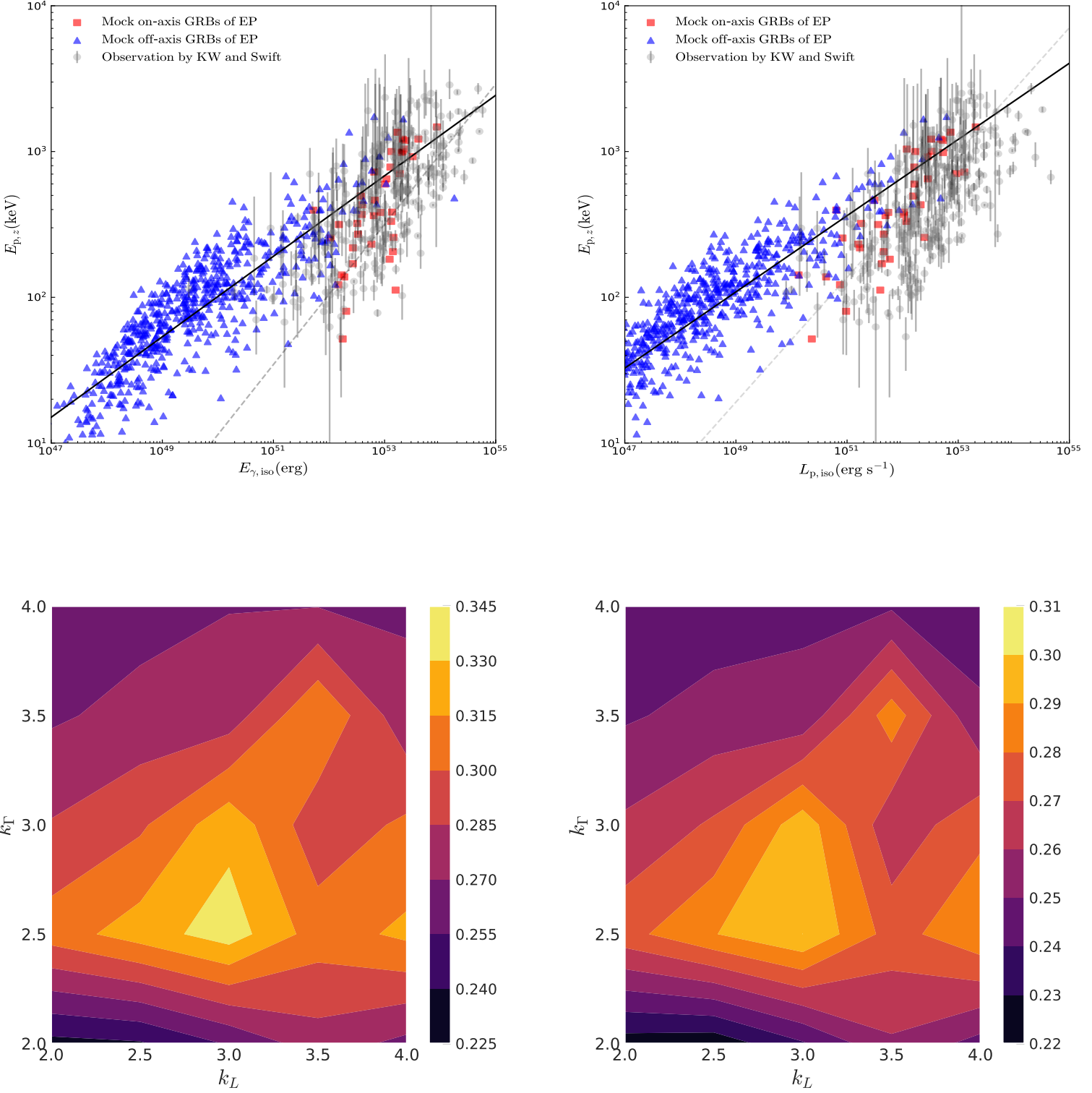


**Figure 9.** Slopes of the Amati and Yonetoku relations predicted by Monte Carlo simulations for EP GRBs. Upper left and right panels: The distribution of mock LGRBs of EP in the  $L_{p,\text{iso}}-E_{p,z}$  and  $E_{\gamma,\text{iso}}-E_{p,z}$  planes. The grey circle dots represent observed LGRBs from Tsvetkova et al. (2021), and the red and blue triangular dots show our mock results for EP LGRBs. The solid line and the dashed line correspond to the best-fit result for mock and observed samples, with the indices  $k_L$  and  $k_T$  fixed at 4. Lower left and right panels: The dependence of the slopes of the Amati (left) and Yonetoku (right) relations for EP LGRBs on the jet structures.

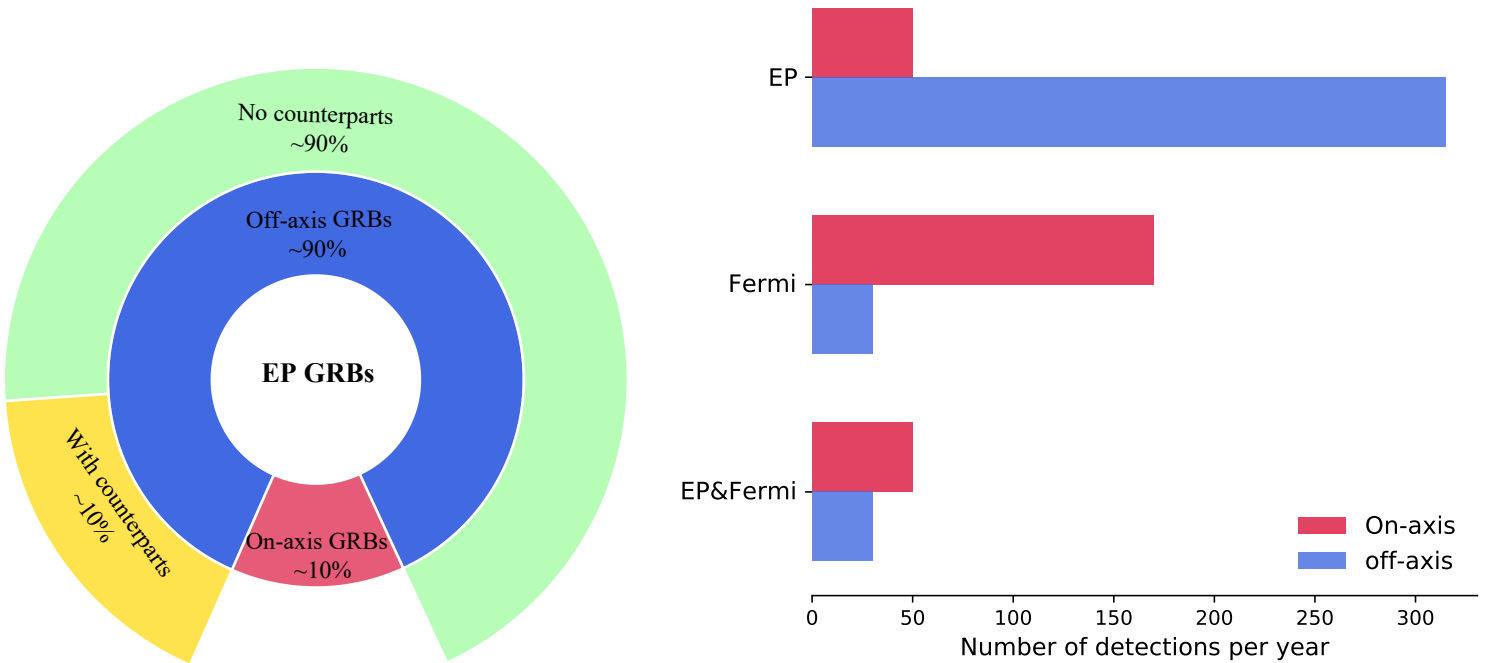


**Figure 10.** Left panel: The estimated distribution of different components in the LGRB sample observed by EP. The inner ring shows the proportion of the off-axis LGRBs (red) and the on-axis LGRBs (blue) among the EP GRBs. The outer ring shows the proportion of bursts with (yellow) and without (green) gamma-ray counterparts among the off-axis GRBs. Right panel: The estimated detection rates of the on-axis (red) or off-axis GRBs (blue) for EP, *Fermi*, and the joint of EP and *Fermi*.

1 We appreciate Bing Zhang for constructive suggestions.  
 2 We also thank Chen-Ran Hu for the helpful discussion.  
 3 This work is based on data obtained with Einstein Probe,  
 4 a space mission supported by Strategic Priority Program on Space Science of Chinese Academy of Sciences,  
 5 in collaboration with ESA, MPE and CNES (Grant No. XDA15310000). This study is partially supported by the National Natural Science Foundation of China (grant Nos. 12273113, 12321003, 12233002, 12393812, 12393813), the National SKA Program of China (grant Nos. 2022SKA0130100, 2020SKA0120300, 2020SKA0120302), the International Partnership Program of Chinese Academy of Sciences for Grand Challenges (114332KYSB20210018), the National Key R&D Program of China (2021YFA0718500), the Strategic Priority Research Program of the Chinese Academy of Sciences (grant No. XDB0550400). Jin-Jun Geng acknowledges support from the Youth Innovation Promotion Association (2023331). Hao-Xuan Gao acknowledges support from Jiangsu Funding Program for Excellent Post-doctoral Talent. Yong-Feng Huang also acknowledges the support from the Xinjiang Tianchi Program.

## REFERENCES

Alexander, K. D., Margutti, R., Blanchard, P. K., et al. 2018, *The Astrophysical Journal Letters*, 863, L18, doi: [10.3847/2041-8213/aad637](https://doi.org/10.3847/2041-8213/aad637)

Aloy, M. A., Janka, H. T., & Müller, E. 2005, *A&A*, 436, 273, doi: [10.1051/0004-6361:20041865](https://doi.org/10.1051/0004-6361:20041865)

Amati, L. 2006, *MNRAS*, 372, 233, doi: [10.1111/j.1365-2966.2006.10840.x](https://doi.org/10.1111/j.1365-2966.2006.10840.x)

Amati, L., Frontera, F., Tavani, M., et al. 2002, *A&A*, 390, 81, doi: [10.1051/0004-6361:20020722](https://doi.org/10.1051/0004-6361:20020722)

Band, D., Matteson, J., Ford, L., et al. 1993, *ApJ*, 413, 281, doi: [10.1086/172995](https://doi.org/10.1086/172995)

Beloborodov, A. M. 2010, *MNRAS*, 407, 1033, doi: [10.1111/j.1365-2966.2010.16770.x](https://doi.org/10.1111/j.1365-2966.2010.16770.x)

Berger, E. 2014, *ARA&A*, 52, 43, doi: [10.1146/annurev-astro-081913-035926](https://doi.org/10.1146/annurev-astro-081913-035926)

Bernardini, M. G., Campana, S., Ghisellini, G., et al. 2013, *ApJ*, 775, 67, doi: [10.1088/0004-637X/775/1/67](https://doi.org/10.1088/0004-637X/775/1/67)

Blandford, R. D., & Znajek, R. L. 1977, *MNRAS*, 179, 433, doi: [10.1093/mnras/179.3.433](https://doi.org/10.1093/mnras/179.3.433)

Bloom, J. S., Frail, D. A., & Sari, R. 2001, *The Astronomical Journal*, 121, 2879, doi: [10.1086/321093](https://doi.org/10.1086/321093)

Bromberg, O., Nakar, E., Piran, T., & Sari, R. 2011, *ApJ*, 740, 100, doi: [10.1088/0004-637X/740/2/100](https://doi.org/10.1088/0004-637X/740/2/100)

Burgess, J. M., Bégué, D., Greiner, J., et al. 2020, *Nature Astronomy*, 4, 174, doi: [10.1038/s41550-019-0911-z](https://doi.org/10.1038/s41550-019-0911-z)

Burlon, D., Ghirlanda, G., Ghisellini, G., et al. 2008, *ApJL*, 685, L19, doi: [10.1086/592350](https://doi.org/10.1086/592350)

Cheng, H. Q., Wang, W. X., Yuan, W., et al. 2024, *GRB Coordinates Network*, 36138, 1

Dado, S., & Dar, A. 2012, *ApJ*, 749, 100, doi: [10.1088/0004-637X/749/2/100](https://doi.org/10.1088/0004-637X/749/2/100)

Dai, Z. G., & Lu, T. 2001, *The Astrophysical Journal*, 551, 249, doi: [10.1086/320056](https://doi.org/10.1086/320056)

Daigne, F., Bošnjak, Ž., & Dubus, G. 2011, *A&A*, 526, A110, doi: [10.1051/0004-6361/201015457](https://doi.org/10.1051/0004-6361/201015457)

Daigne, F., Rossi, E. M., & Mochkovitch, R. 2006, *MNRAS*, 372, 1034, doi: [10.1111/j.1365-2966.2006.10837.x](https://doi.org/10.1111/j.1365-2966.2006.10837.x)

Demianski, M., Piedipalumbo, E., Sawant, D., & Amati, L. 2017, *A&A*, 598, A112, doi: [10.1051/0004-6361/201628909](https://doi.org/10.1051/0004-6361/201628909)

Derishev, E. V., Kocharovsky, V. V., & Kocharovsky, V. V. 2001, *A&A*, 372, 1071, doi: [10.1051/0004-6361:20010586](https://doi.org/10.1051/0004-6361:20010586)

Eichler, D., & Levinson, A. 2004, *ApJL*, 614, L13, doi: [10.1086/425310](https://doi.org/10.1086/425310)

Eichler, D., Livio, M., Piran, T., & Schramm, D. N. 1989, *Nature*, 340, 126, doi: [10.1038/340126a0](https://doi.org/10.1038/340126a0)

Firmani, C., Avila-Reese, V., Ghisellini, G., & Tutukov, A. V. 2004, *ApJ*, 611, 1033, doi: [10.1086/422186](https://doi.org/10.1086/422186)

Gao, H.-X., Geng, J.-J., & Huang, Y.-F. 2021, *Astronomy & Astrophysics*, 656, A134, doi: [10.1051/0004-6361/202141647](https://doi.org/10.1051/0004-6361/202141647)

Gao, H.-X., Geng, J.-J., Sun, T.-R., et al. 2024, *The Astrophysical Journal*, 971, 81, doi: [10.3847/1538-4357/ad5443](https://doi.org/10.3847/1538-4357/ad5443)

Gao, H.-X., Geng, J.-J., Hu, L., et al. 2022, *MNRAS*, 516, 453, doi: [10.1093/mnras/stac2215](https://doi.org/10.1093/mnras/stac2215)

Geng, J.-J., Huang, Y.-F., Wu, X.-F., Song, L.-M., & Zong, H.-S. 2018a, *ApJ*, 862, 115, doi: [10.3847/1538-4357/aaecd05](https://doi.org/10.3847/1538-4357/aaecd05)

Geng, J.-J., Huang, Y.-F., Wu, X.-F., Zhang, B., & Zong, H.-S. 2018b, *ApJS*, 234, 3, doi: [10.3847/1538-4365/aa9e84](https://doi.org/10.3847/1538-4365/aa9e84)

Geng, J. J., Wu, X. F., Huang, Y. F., Li, L., & Dai, Z. G. 2016a, *ApJ*, 825, 107, doi: [10.3847/0004-637X/825/2/107](https://doi.org/10.3847/0004-637X/825/2/107)

Geng, J.-J., Zhang, B., & Kuiper, R. 2016b, *ApJ*, 833, 116, doi: [10.3847/1538-4357/833/1/116](https://doi.org/10.3847/1538-4357/833/1/116)

Granot, J., Guetta, D., & Gill, R. 2017, *ApJL*, 850, L24, doi: [10.3847/2041-8213/aa991d](https://doi.org/10.3847/2041-8213/aa991d)

Granot, J., Panaiteescu, A., Kumar, P., & Woosley, S. E. 2002, *ApJL*, 570, L61, doi: [10.1086/340991](https://doi.org/10.1086/340991)

Guetta, D., & Della Valle, M. 2007, *ApJL*, 657, L73, doi: [10.1086/511417](https://doi.org/10.1086/511417)

Ho, A. Y., Perley, D. A., Yao, Y., et al. 2022, *The Astrophysical Journal*, 938, 85, doi: [10.3847/1538-4357/ac8bd0](https://doi.org/10.3847/1538-4357/ac8bd0)

Hu, Y.-D., Liang, E.-W., Xi, S.-Q., et al. 2014, *ApJ*, 789, 145, doi: [10.1088/0004-637X/789/2/145](https://doi.org/10.1088/0004-637X/789/2/145)

Huang, Y. F., Dai, Z. G., & Lu, T. 2002, *MNRAS*, 332, 735, doi: [10.1046/j.1365-8711.2002.05334.x](https://doi.org/10.1046/j.1365-8711.2002.05334.x)

Kasliwal, M. M., Nakar, E., Singer, L. P., et al. 2017, *Science*, 358, 1559, doi: [10.1126/science.aap9455](https://doi.org/10.1126/science.aap9455)

Kathirgamaraju, A., Barniol Duran, R., & Giannios, D. 2018, *MNRAS*, 473, L121, doi: [10.1093/mnrasl/slx175](https://doi.org/10.1093/mnrasl/slx175)

Kocevski, D. 2012, *ApJ*, 747, 146, doi: [10.1088/0004-637X/747/2/146](https://doi.org/10.1088/0004-637X/747/2/146)

Koshut, T. M., Kouveliotou, C., Paciesas, W. S., et al. 1995, *ApJ*, 452, 145, doi: [10.1086/176286](https://doi.org/10.1086/176286)

Kouveliotou, C., Meegan, C. A., Fishman, G. J., et al. 1993, *ApJL*, 413, L101, doi: [10.1086/186969](https://doi.org/10.1086/186969)

Kumar, P., & Granot, J. 2003, *ApJ*, 591, 1075, doi: [10.1086/375186](https://doi.org/10.1086/375186)

Kumar, P., & Zhang, B. 2015, *PhR*, 561, 1, doi: [10.1016/j.physrep.2014.09.008](https://doi.org/10.1016/j.physrep.2014.09.008)

Lamb, G. P., & Kobayashi, S. 2017, *MNRAS*, 472, 4953, doi: [10.1093/mnras/stx2345](https://doi.org/10.1093/mnras/stx2345)

Lan, G.-X., Wei, J.-J., Zeng, H.-D., Li, Y., & Wu, X.-F. 2021, *MNRAS*, 508, 52, doi: [10.1093/mnras/stab2508](https://doi.org/10.1093/mnras/stab2508)

Lazzati, D. 2005, *MNRAS*, 357, 722, doi: [10.1111/j.1365-2966.2005.08687.x](https://doi.org/10.1111/j.1365-2966.2005.08687.x)

Lazzati, D., Perna, R., Morsony, B. J., et al. 2018, *PhRvL*, 120, 241103, doi: [10.1103/PhysRevLett.120.241103](https://doi.org/10.1103/PhysRevLett.120.241103)

Levinson, A., & Eichler, D. 2003, *ApJL*, 594, L19, doi: [10.1086/378487](https://doi.org/10.1086/378487)

Li, L.-B., Geng, J.-J., Huang, Y.-F., & Li, B. 2019, *ApJ*, 880, 39, doi: [10.3847/1538-4357/ab275d](https://doi.org/10.3847/1538-4357/ab275d)

Lian, T. Y., Pan, X., Ling, Z. X., et al. 2024, *GRB Coordinates Network*, 36091, 1

Liang, E., Zhang, B., Virgili, F., & Dai, Z. G. 2007, *ApJ*, 662, 1111, doi: [10.1086/517959](https://doi.org/10.1086/517959)

Lipunov, V. M., Postnov, K. A., & Prokhorov, M. E. 2001, *Astronomy Reports*, 45, 236, doi: [10.1134/1.1353364](https://doi.org/10.1134/1.1353364)

Liu, Y., Sun, H., Xu, D., et al. 2024, arXiv e-prints, arXiv:2404.16425, doi: [10.48550/arXiv.2404.16425](https://doi.org/10.48550/arXiv.2404.16425)

Meegan, C. A., Fishman, G. J., Wilson, R. B., et al. 1992, *Nature*, 355, 143, doi: [10.1038/355143a0](https://doi.org/10.1038/355143a0)

Meng, Y.-Z., Geng, J.-J., Zhang, B.-B., et al. 2018, *ApJ*, 860, 72, doi: [10.3847/1538-4357/aac2d9](https://doi.org/10.3847/1538-4357/aac2d9)

Mészáros, P., Rees, M., & Wijers, R. 1999, *New Astronomy*, 4, 303

Mészáros, P., & Rees, M. J. 2000, *ApJ*, 530, 292, doi: [10.1086/308371](https://doi.org/10.1086/308371)

Mészáros, P., Rees, M. J., & Papathanassiou, H. 1994, *ApJ*, 432, 181, doi: [10.1086/174559](https://doi.org/10.1086/174559)

Mészáros, P., Rees, M. J., & Wijers, R. A. M. J. 1998, *ApJ*, 499, 301, doi: [10.1086/305635](https://doi.org/10.1086/305635)

Minaev, P. Y., & Pozanenko, A. S. 2020, *MNRAS*, 492, 1919, doi: [10.1093/mnras/stz3611](https://doi.org/10.1093/mnras/stz3611)

Mochkovitch, R., & Nava, L. 2015, *A&A*, 577, A31, doi: [10.1051/0004-6361/201424490](https://doi.org/10.1051/0004-6361/201424490)

Morsony, B. J., Lazzati, D., & Begelman, M. C. 2010, *ApJ*, 723, 267, doi: [10.1088/0004-637X/723/1/267](https://doi.org/10.1088/0004-637X/723/1/267)

Nagakura, H., Hotokezaka, K., Sekiguchi, Y., Shibata, M., & Ioka, K. 2014, *ApJL*, 784, L28, doi: [10.1088/2041-8205/784/2/L28](https://doi.org/10.1088/2041-8205/784/2/L28)

Nakar, E., & Piran, T. 2016, *The Astrophysical Journal*, 834, 28, doi: [10.3847/1538-4357/834/1/28](https://doi.org/10.3847/1538-4357/834/1/28)

Nava, L., Salvaterra, R., Ghirlanda, G., et al. 2012, *MNRAS*, 421, 1256, doi: [10.1111/j.1365-2966.2011.20394.x](https://doi.org/10.1111/j.1365-2966.2011.20394.x)

Paciesas, W. S., & Fermi GBM Collaboration. 2012, in *American Astronomical Society Meeting Abstracts*, Vol. 219, American Astronomical Society Meeting Abstracts #219, 149.12

Paczynski, B., & Xu, G. 1994, *ApJ*, 427, 708, doi: [10.1086/174178](https://doi.org/10.1086/174178)

Pe'er, A., Mészáros, P., & Rees, M. J. 2006, *ApJ*, 642, 995, doi: [10.1086/501424](https://doi.org/10.1086/501424)

Pescalli, A., Ghirlanda, G., Salafia, O. S., et al. 2015, MNRAS, 447, 1911, doi: [10.1093/mnras/stu2482](https://doi.org/10.1093/mnras/stu2482)

Petrosian, V., Kitanidis, E., & Kocevski, D. 2015, ApJ, 806, 44, doi: [10.1088/0004-637X/806/1/44](https://doi.org/10.1088/0004-637X/806/1/44)

Piran, T. 2004, Reviews of Modern Physics, 76, 1143, doi: [10.1103/RevModPhys.76.1143](https://doi.org/10.1103/RevModPhys.76.1143)

Preece, R. D., Briggs, M. S., Mallozzi, R. S., et al. 1998, ApJL, 506, L23, doi: [10.1086/311644](https://doi.org/10.1086/311644)

Qin, Y.-P., & Chen, Z.-F. 2013, MNRAS, 430, 163, doi: [10.1093/mnras/sts547](https://doi.org/10.1093/mnras/sts547)

Ramirez-Ruiz, E., Granot, J., Kouveliotou, C., et al. 2005, ApJL, 625, L91, doi: [10.1086/431237](https://doi.org/10.1086/431237)

Rees, M. J., & Mészáros, P. 1994, ApJL, 430, L93, doi: [10.1086/187446](https://doi.org/10.1086/187446)

—. 2005, ApJ, 628, 847, doi: [10.1086/430818](https://doi.org/10.1086/430818)

Rhoads, J. E. 1997, ApJL, 487, L1, doi: [10.1086/310876](https://doi.org/10.1086/310876)

Rossi, E., Lazzati, D., & Rees, M. J. 2002, MNRAS, 332, 945, doi: [10.1046/j.1365-8711.2002.05363.x](https://doi.org/10.1046/j.1365-8711.2002.05363.x)

Rybicki, G. B., & Lightman, A. P. 1979, Radiative processes in astrophysics

Ryde, F., Pe'er, A., Nymark, T., et al. 2011, MNRAS, 415, 3693, doi: [10.1111/j.1365-2966.2011.18985.x](https://doi.org/10.1111/j.1365-2966.2011.18985.x)

Sakamoto, T., Barthelmy, S. D., Barbier, L., et al. 2008, ApJS, 175, 179, doi: [10.1086/523646](https://doi.org/10.1086/523646)

Sakamoto, T., Barthelmy, S. D., Baumgartner, W. H., et al. 2011, ApJS, 195, 2, doi: [10.1088/0067-0049/195/1/2](https://doi.org/10.1088/0067-0049/195/1/2)

Salvaterra, R., & Chincarini, G. 2007, ApJL, 656, L49, doi: [10.1086/512606](https://doi.org/10.1086/512606)

Salvaterra, R., Della Valle, M., Campana, S., et al. 2009, Nature, 461, 1258, doi: [10.1038/nature08445](https://doi.org/10.1038/nature08445)

Salvaterra, R., Campana, S., Vergani, S. D., et al. 2012, ApJ, 749, 68, doi: [10.1088/0004-637X/749/1/68](https://doi.org/10.1088/0004-637X/749/1/68)

Spruit, H. C., Daigne, F., & Drenkhahn, G. 2001, A&A, 369, 694, doi: [10.1051/0004-6361:20010131](https://doi.org/10.1051/0004-6361:20010131)

Sun, H., Li, W. X., Liu, L. D., et al. 2024a, arXiv e-prints, arXiv:2410.02315, doi: [10.48550/arXiv.2410.02315](https://doi.org/10.48550/arXiv.2410.02315)

Sun, T.-R., Geng, J.-J., Yan, J.-Z., et al. 2024b, ApJL in press, arXiv:2409.17983, doi: [10.48550/arXiv.2409.17983](https://doi.org/10.48550/arXiv.2409.17983)

Tarnopolski, M. 2016, MNRAS, 458, 2024, doi: [10.1093/mnras/stw429](https://doi.org/10.1093/mnras/stw429)

Tavani, M. 1996, ApJ, 466, 768, doi: [10.1086/177551](https://doi.org/10.1086/177551)

Tsvetkova, A., Frederiks, D., Golenetskii, S., et al. 2017, ApJ, 850, 161, doi: [10.3847/1538-4357/aa96af](https://doi.org/10.3847/1538-4357/aa96af)

Tsvetkova, A., Frederiks, D., Svinkin, D., et al. 2021, ApJ, 908, 83, doi: [10.3847/1538-4357/abd569](https://doi.org/10.3847/1538-4357/abd569)

Uhm, Z. L., & Zhang, B. 2014, Nature Physics, 10, 351, doi: [10.1038/nphys2932](https://doi.org/10.1038/nphys2932)

—. 2016, ApJL, 824, L16, doi: [10.3847/2041-8205/824/1/L16](https://doi.org/10.3847/2041-8205/824/1/L16)

Uhm, Z. L., Zhang, B., & Racusin, J. 2018, ApJ, 869, 100, doi: [10.3847/1538-4357/aaeb30](https://doi.org/10.3847/1538-4357/aaeb30)

van Putten, M. H. P. M., & Levinson, A. 2003, The Astrophysical Journal, 584, 937, doi: [10.1086/345900](https://doi.org/10.1086/345900)

Vlahakis, N., Peng, F., & Königl, A. 2003, ApJL, 594, L23, doi: [10.1086/378580](https://doi.org/10.1086/378580)

Wanderman, D., & Piran, T. 2010, MNRAS, 406, 1944, doi: [10.1111/j.1365-2966.2010.16787.x](https://doi.org/10.1111/j.1365-2966.2010.16787.x)

Wang, X.-G., Zhang, B., Liang, E.-W., et al. 2018, ApJ, 859, 160, doi: [10.3847/1538-4357/aabc13](https://doi.org/10.3847/1538-4357/aabc13)

Wichern, H. C. I., Ravasio, M. E., Jonker, P. G., et al. 2024, A&A, 690, A101, doi: [10.1051/0004-6361/202450116](https://doi.org/10.1051/0004-6361/202450116)

Xiao, D., Liu, L.-D., Dai, Z.-G., & Wu, X.-F. 2017, ApJL, 850, L41, doi: [10.3847/2041-8213/aa9b2b](https://doi.org/10.3847/2041-8213/aa9b2b)

Xu, F., Huang, Y.-F., Geng, J.-J., et al. 2023, A&A, 673, A20, doi: [10.1051/0004-6361/202245414](https://doi.org/10.1051/0004-6361/202245414)

Yamazaki, R., Ioka, K., & Nakamura, T. 2004, ApJL, 606, L33, doi: [10.1086/421084](https://doi.org/10.1086/421084)

Yin, Y.-H. I., Zhang, B.-B., Yang, J., et al. 2024, arXiv e-prints, arXiv:2407.10156, doi: [10.48550/arXiv.2407.10156](https://doi.org/10.48550/arXiv.2407.10156)

Yonetoku, D., Murakami, T., Nakamura, T., et al. 2004, ApJ, 609, 935, doi: [10.1086/421285](https://doi.org/10.1086/421285)

Yu, H., Wang, F. Y., Dai, Z. G., & Cheng, K. S. 2015, ApJS, 218, 13, doi: [10.1088/0067-0049/218/1/13](https://doi.org/10.1088/0067-0049/218/1/13)

Yuan, W., Zhang, C., Chen, Y., & Ling, Z. 2022, The Einstein Probe Mission, ed. C. Bambi & A. Santangelo (Singapore: Springer Nature Singapore), 1–30, doi: [10.1007/978-981-16-4544-0\\_151-1](https://doi.org/10.1007/978-981-16-4544-0_151-1)

Yuan, W., Zhang, C., Ling, Z., et al. 2024, in Space Telescopes and Instrumentation 2024: Ultraviolet to Gamma Ray, ed. J.-W. A. den Herder, S. Nikzad, & K. Nakazawa, Vol. 13093, International Society for Optics and Photonics (SPIE), 130931C, doi: [10.1117/12.3023595](https://doi.org/10.1117/12.3023595)

Zhang, B. 2018, The Physics of Gamma-Ray Bursts (Cambridge: Cambridge Univ. Press), doi: [10.1017/9781139226530](https://doi.org/10.1017/9781139226530)

Zhang, B., & Mészáros, P. 2002a, ApJ, 571, 876, doi: [10.1086/339981](https://doi.org/10.1086/339981)

—. 2002b, ApJ, 581, 1236, doi: [10.1086/344338](https://doi.org/10.1086/344338)

Zhang, B., & Yan, H. 2011a, ApJ, 726, 90, doi: [10.1088/0004-637X/726/2/90](https://doi.org/10.1088/0004-637X/726/2/90)

—. 2011b, ApJ, 726, 90, doi: [10.1088/0004-637X/726/2/90](https://doi.org/10.1088/0004-637X/726/2/90)

Zhang, F.-W., Shao, L., Yan, J.-Z., & Wei, D.-M. 2012, ApJ, 750, 88, doi: [10.1088/0004-637X/750/2/88](https://doi.org/10.1088/0004-637X/750/2/88)

Zhang, W., Woosley, S. E., & MacFadyen, A. I. 2003, ApJ, 586, 356, doi: [10.1086/367609](https://doi.org/10.1086/367609)

Zhang, W. J., Mao, X., Zhang, W. D., et al. 2024, GRB Coordinates Network, 35931, 1

Zhang, Y., Geng, J.-J., & Huang, Y.-F. 2019, ApJ, 877, 89,  
doi: [10.3847/1538-4357/ab1b10](https://doi.org/10.3847/1538-4357/ab1b10)

Zhao, X., Li, Z., Liu, X., et al. 2014, ApJ, 780, 12,  
doi: [10.1088/0004-637X/780/1/12](https://doi.org/10.1088/0004-637X/780/1/12)

Zhou, H., Chen, W., Sun, H., et al. 2024a, GRB  
Coordinates Network, 36691, 1

Zhou, H., Wang, W. X., Hu, J. W., et al. 2024b, GRB  
Coordinates Network, 36997, 1